A Predictive Methodology for Delamination Growth in Laminated Composites

Part I: Theoretical Development and Preliminary Experimental Results

April 1998

Final Report

U.S. Department of Transportation
Federal Aviation Administration

NOTICE

This document is disseminated under the sponsorship of the U.S. Department of Transportation in the interest of information exchange. The United States Government assumes no liability for the contents or use thereof. The United States Government does not endorse products or manufacturers. Trade or manufacturer's names appear herein solely because they are considered essential to the objective of this report.

1. Report No.	2. Government Accession No.	3. Recipient's Catalog No.
DOT/FAA/AR-97/87		

4. Title and Subtitle	5. Report Date
A PREDICTIVE METHODOLOGY FOR DELAMINATION GROWTH IN LAMINATED COMPOSITES	April 1998
Part I: Theoretical Development and Preliminary Experimental Results	6. Performing Organization Code

7. Author(s)	8. Performing Organization Report No.
Barry D. Davidson	

9. Performing Organization Name and Address	10. Work Unit No. (TRAIS)
Department of Mechanical, Aerospace and Manufacturing Engineering Syracuse University Syracuse, NY 13244	
	11. Contract or Grant No.
	94-G-022

12. Sponsoring Agency Name and Address	13. Type of Report and Period Covered
U.S. Department of Transportation Federal Aviation Administration Office of Aviation Research Washington, DC 20591	Final Report
	14. Sponsoring Agency Code
	AAR-431

15. Supplementary Notes
FAA William J. Hughes Technical Center Technical Monitor: Peter Shyprykevich

16. Abstract

A methodology is presented for the prediction of delamination growth in laminated structures. The methodology is aimed at overcoming computational difficulties in the determination of energy release rate and mode mix. It also addresses the issue that many laminated composites exhibit large-scale crack tip damage zones and, as such, a singular field-based mode mix decomposition may not accurately account for the dependence of toughness on the loading. In the methodology, the toughness versus mode mix relation, and the definition of mode mix itself, is first determined experimentally. The definition of mode mix is found from the results of a series of delamination toughness tests and is obtained within the construct of a crack tip element analysis. Next, the structure of interest is analyzed using the crack tip element analysis and the experimentally determined definition of mode mix, and delamination growth assessments are performed. This approach also obviates the need for locally detailed two- and three-dimensional finite element analyses.

17. Key Words	18. Distribution Statement
Delamination, Fracture, Graphite/Epoxy, Mixed-mode, Crack tip element, Finite element	This document is available to the public through the National Technical Information Service (NTIS), Springfield, Virginia 22161.

19. Security Classif. (of this report)	20. Security Classif. (of this page)	21. No. of Pages	22. Price
Unclassified	Unclassified	50	

Form DOT F1700.7 (8-72)   Reproduction of completed page authorized

ACKNOWLEDGEMENTS

TABLE OF CONTENTS

LIST OF FIGURES

LIST OF TABLES

EXECUTIVE SUMMARY

Due to their high strength and stiffness-to-weight ratios, laminated composite materials are increasingly being used in the aerospace industry. However, due to the lack of through-the-thickness reinforcement, structures made from these materials are highly susceptible to failures caused by delamination growth. Therefore, in order to maximize durability and damage tolerance, a structure's resistance to delamination should be addressed within the design process. By gaining an understanding of what causes delaminations to initiate and grow, a predictive methodology can be developed and used by designers to select structural configurations where the propensity for delamination is minimized. In addition, such a predictive methodology would be useful for assessing the criticality of service-induced delaminations that have been detected.

The current, state-of-the-art methodology for predicting delamination growth is lacking in three respects. First, it is extremely labor intensive, both in terms of man-hours and computational effort. For this reason alone, the aerospace industry has been reluctant to adopt it. Second, experimental verifications of the methodology are almost nonexistent. Third, and perhaps most importantly, the methodology that is used for laminated composites is primarily a carryover from that used for metals. However, the mechanisms that occur during delamination growth in composites are often quite different from those that occur during crack propagation in metals, and in certain instances the current approach is not appropriate. This issue is not generally recognized, however, precisely because there has not been a great deal of experimental verification of the state-of-the-art method.

This report describes a predictive methodology for delamination growth that overcomes all of the above drawbacks of the state-of-the-art approach. First, the method is simple to implement for most practical geometries. Due to this simplicity, a large number of locations can be examined for the propensity for delaminations to grow. Thus, the method can be applied during the design process or for discrete damages found from service usage. Second, the method has been verified by an extensive amount of testing. Third, the theory utilizes assumptions that are consistent with the mechanics of the growth of delaminations in laminated composites, and failure predictions by this new method agree quite well with preliminary experimental results. Thus, there is a great expectation that this new methodology will provide a powerful tool that can rapidly be integrated into current engineering environments.

This report is envisioned to be the first of a two-part series. In this first part, the theoretical development of the method is presented, and experimental results are shown for a single material for a variety of relatively standard test geometries. In the second part, the method will be applied to other materials as well as geometries that are more representative of those found in typical aircraft structures.

1. INTRODUCTION.

Despite the relatively widespread attention given to the problem of delamination in laminated composites, significant fundamental as well as computational problems still remain with most current approaches to predict this failure mode. In order to assess for possible delamination growth in a given structural geometry, it is generally accepted that one can analytically or numerically determine the total strain energy release rate along a delamination front and compare these results, at the appropriate mode mix, to an experimentally determined toughness [1-3]. Here, the term "mode mix" is used to denote the relative percentages of the mode I (opening mode) and mode II (shearing mode) components of the total energy release rate. However, there are significant problems with this procedure, most notably in the determination of mode mix and in the associated determination of toughness. For example, for most practical geometries, mode mixity determination is an extremely computationally intensive procedure and requires very detailed two- or three-dimensional finite element analyses of the crack tip region for each delamination location and loading of interest. [1] Thus, in many instances, computational requirements alone make it relatively impractical to make delamination growth assessments at a large number of locations. Additional difficulties involve the definition of mode mix. If a classical, linear elastic fracture mechanics definition is adopted, then for most cases of practical interest where delaminations occur between plies with dissimilar orientations, a mode mix based on conventional energy release rate (ERR) components cannot be defined. In these instances, a linear elastic analysis that models individual plies as equivalent homogeneous layers will predict that an oscillatory stress singularity exists at the delamination front. This oscillatory field complicates the implementation of any predictive methodology. Finally, even if one chooses to go forward and to perform the necessary computations, recent experimental evidence [3-6] indicates that a predictive methodology using ERR and the singular field-based definition of mode mix may be inaccurate for many fibrous composites. This is because many composites exhibit large damage zones in the vicinity of the delamination front, in which case the concept of a singular zone does not apply. Thus, it is observed experimentally that the toughness of most laminated composites is dependent upon the type of loading; however, for use in a predictive methodology, the singular field-based definition of mode mix is often not appropriate.

In this report, an engineering methodology is described for use in making delamination growth assessments in laminated composite structures. The methodology contains two primary components. First, the toughness versus mode mix relation, and the definition of mode mix itself, is determined experimentally. The definition of mode mix that is sought is the one that, when applied to all experimental results, produces a single-valued toughness versus mode mix curve. That is, the definition must be such that different geometries that are predicted to be at the same mode mix display the same toughness. The mode mix definition is found from the results of a series of delamination toughness tests and is obtained within the construct of a crack tip element analysis. This approach allows for the possibility that the singular field-based decomposition is valid; it also allows for the possibility that an alternative definition is valid. This alternative definition is based on parameters that uniquely define the loading at the crack tip but which are insensitive to the details of the near-tip damage. The second component of the methodology described herein consists of analyzing the structure of interest and assessing delamination growth. This is also done using the crack tip element analysis and incorporates the

experimentally determined definition of mode mix. Note that this approach obviates the need for locally detailed two- and three-dimensional finite element analyses.

2. CRACK TIP ELEMENT ANALYSIS.

2.1 TOTAL ENERGY RELEASE RATE.

Consider the crack tip element of figure 1. This element is assumed to represent a three-dimensional portion of the crack tip region in a general interfacial fracture problem. It is assumed that the crack lies locally in the x-y plane at constant z. The crack front may be straight or curved; however, the length of the element in the y direction is assumed to be sufficiently short such that there is no significant variation in the loading and in the orientation of the edges of the element with respect to y. It is further assumed that the lengths of the cracked and uncracked regions comprising the element are large with respect to their thicknesses but are sufficiently small such that geometric nonlinearities are negligible. Thus, classical plate theory (CPT) may be used to predict the overall deformations and strain energies of the element. The derivation below essentially follows that which is presented in reference 1. For simplicity of presentation, it is assumed that the element is in a state of plane stress or plane strain with respect to the y coordinate direction. The three-dimensional analysis is described in reference 7 and is presented in detail in reference 8. For later use within this report, some specific results for the three-dimensional case are taken from reference 8 and are given following the derivation below.
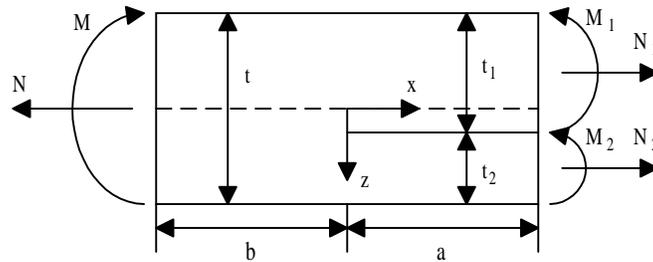
FIGURE 1. CRACK TIP ELEMENT AND LOCAL LOADING

In classical plate theory, deformations are defined entirely by midsurface strains and curvatures. For the uncracked portion of the element, the equations relating these midsurface strains and curvatures to the load and moment resultants are given by

$$N = A\varepsilon^{o} + B\kappa$$
$$M = B\varepsilon^{o} + D\kappa$$

(1)

Or, in their inverted form

$$\varepsilon^{o} = A'N + B'M$$
$$\kappa = B'N + D'M$$

(2)

where ε^o is the strain in the x direction and κ is the plate theory curvature ($= -\partial^2 w/\partial x^2$) of the uncracked region. N and M are the load and moment resultants per unit width, respectively, and are defined positive as shown in figure 1. The coupling modulus, B, and compliance, B′, will be zero for problems in which the uncracked region possesses midplane symmetry. A homogeneous material is one special case. However, it may be that laminated composites do not possess midplane symmetry and will therefore have nonzero coupling coefficients.

For the region above the crack plane (plate 1) or below the crack plane (plate 2), the midsurface strains and curvatures are related to the load and moment resultants by

$$N_i = A_i \varepsilon_i^o + B_i \kappa_i, \qquad i = 1,2$$
$$M_i = B_i \varepsilon_i^o + D_i \kappa_i, \qquad i = 1,2 \tag{3}$$

Or, in their inverted form

$$\varepsilon_i^o = A_i' N_i + B_i' M_i, \qquad i = 1,2$$
$$\kappa_i = B_i' N_i + D_i' M_i, \qquad i = 1,2 \tag{4}$$

where ε_i^o is the midplane strain in the x direction in plate i, κ_i is the curvature in the x direction of plate i, and N_1, N_2, M_1, and M_2 are positive as shown in figure 1. The subscript i is not summed in equations 3 and 4.

It has been shown [1, 7] that the loading on the crack tip element which produces the stress singularity can be fully characterized in terms of a concentrated crack tip force, N_c, and moment, M_c. The concentrated crack tip force and moment are found by enforcing the condition that the displacements of the upper and lower plates be compatible along the crack plane over -b < x < 0. The ERR of the crack tip element is obtained through a modified virtual crack closure method and may be expressed in terms of N_c and M_c, rather than the four independent quantities N_1, N_2, M_1, and M_2. This gives [1, 7]

$$G = \frac{1}{2}\left(c_1 N_c^2 + c_2 M_c^2 + 2\sqrt{c_1 c_2}\, N_c M_c \sin \Gamma\right) \tag{5}$$

where
$$\sin \Gamma = \frac{c_{12}}{\sqrt{c_1 c_2}} \tag{6}$$

and Γ has been introduced for later use. Also,

$$c_1 = A_1' + A_2' + B_1' t_1 - B_2' t_2 + \frac{D_1' t_1^2}{4} + \frac{D_2' t_2^2}{4}$$
$$c_2 = D_1' + D_2' \tag{7}$$
$$c_{12} = \frac{D_2' t_2}{2} - \frac{D_1' t_1}{2} - B_1' - B_2'$$

3

The concentrated crack tip force and moment are given by

$$N_c = -N_1 + a_{11}N + a_{12}M \tag{8}$$

and

$$M_c = M_1 - \frac{N_1 t_1}{2} + \left(\frac{a_{11}t_1}{2} - a_{21} \right)N + \left(\frac{a_{12}t_1}{2} - a_{22} \right)M \tag{9}$$

where

$$a_{11} = A_1 A' + \left(B_1 - \frac{A_1 t_2}{2} \right)B'$$

$$a_{12} = A_1 B' + \left(B_1 - \frac{A_1 t_2}{2} \right)D'$$

$$\tag{10}$$

$$a_{21} = B_1 A' + \left(D_1 - \frac{B_1 t_2}{2} \right)B'$$

$$a_{22} = B_1 B' + \left(D_1 - \frac{B_1 t_2}{2} \right)D'$$

and t_1 and t_2 are the thicknesses of plates 1 and 2 as shown in figure 1.

2.2 MODE DECOMPOSITION ACCORDING TO THE CLASSICAL DEFINITION.

To decompose the total ERR, equation 5, into its mode I and mode II components, G is first related to the modulus of the in-plane complex stress-intensity factor, K. Next, K is written in terms of N_c and M_c. Since this expression must be linear, two unknown constants of proportionality are introduced. These may be determined, apart from a phase angle, by equating the expression for G given by equation 5 to that obtained when G is expressed in terms of K and K is expressed in terms of N_c and M_c. This gives the following expression for the stress-intensity factor [1]

$$K = \left(\frac{2}{H_{11}} \right)^{\frac{1}{2}} \cosh \pi\varepsilon \left(iN_c \sqrt{c_1} + M_c \sqrt{c_2} e^{i\Gamma} \right) L^{-i\varepsilon} e^{i\Omega} \tag{11}$$

Here, Ω is a yet-to-be-determined mode mix parameter and ε is the bimaterial constant, given by

$$\varepsilon = \left(\frac{1}{2\pi} \right) \ln \left[\frac{(1-\beta)}{(1+\beta)} \right] \tag{12}$$

which vanishes when the material properties immediately above and below the crack plane are the same. In this case, the stress field is found to have an inverse-square root singularity, whereas when $\varepsilon \neq 0$ the singularity is predicted to be oscillatory. [1] Notice that $\varepsilon = 0$ when $\beta = 0$, where β is a generalization of one of Dundurs' parameters [9] for isotropic materials and is given by [1, 10]

$$\beta = \left(\left[(s_{11}s_{33})^{1/2} + s_{13}\right]_2 - \left[(s_{11}s_{33})^{1/2} + s_{13}\right]_1\right)(H_{11}H_{33})^{-1/2} \qquad (13)$$

where
$$H_{11} = \left[2n\lambda^{1/4}(s_{11}s_{33})^{1/2}\right]_1 + \left[2n\lambda^{1/4}(s_{11}s_{33})^{1/2}\right]_2 \qquad (14)$$

and
$$H_{33} = \left[2n\lambda^{-1/4}(s_{11}s_{33})^{1/2}\right]_1 + \left[2n\lambda^{-1/4}(s_{11}s_{33})^{1/2}\right]_2 \qquad (15)$$

The subscripts 1 and 2 used outside the square brackets in the expressions for β, H_{11}, and H_{33} refer to the materials immediately above and below the crack plane, respectively. In the case of laminated materials, these are the two plies or ply groups bounding the delamination. The nondimensional parameters λ and n are given by

$$\lambda = s_{11} \Big/ s_{33} \qquad (16)$$

and
$$n = \left[\tfrac{1}{2}(1 + \rho)\right]^{1/2} \qquad (17)$$

where
$$\rho = \tfrac{1}{2}(2s_{13} + s_{55})(s_{11}s_{33})^{-1/2} \qquad (18)$$

Material compliances are defined in the conventional sense; that is, the stress-strain relations for either material (immediately above or below the crack plane) are assumed to be of the form

$$\varepsilon_i = s_{ij}\sigma_j \qquad (19)$$

Standard contracted notation is used. [11] Using s_{ij} as defined in equation 19 gives plane stress results; plane strain values are obtained by replacing s_{ij} by s'_{ij}, where

$$s'_{ij} = s_{ij} - s_{i2}s_{j2}\Big/ s_{22} \qquad (20)$$

To decompose the stress-intensity factor, equation 11, into its mode I and mode II components, the following definition is used [1, 12]

$$K\hat{L}^{i\varepsilon} = K_I + iK_{II} \qquad (21)$$

where $\hat{L}$ is a fixed dimension that does not scale with the size of the body and is used for fracture characterization of that interface. [1, 12] Using the above definitions, the in-plane phase angle of the stress-intensity factor, or mode mixity, ψ, is given by

$$\tan\psi = K_{II}\Big/ K_I \qquad (22)$$

Guided by equation 21, the mode I and mode II ERRs are given by [1]

$$G_I = \frac{1}{2}\left[-N_c\sqrt{c_1}\sin\hat{\Omega} + M_c\sqrt{c_2}\cos(\hat{\Omega}+\Gamma)\right]^2 \tag{23}$$

and
$$G_{II} = \frac{1}{2}\left[N_c\sqrt{c_1}\cos\hat{\Omega} + M_c\sqrt{c_2}\sin(\hat{\Omega}+\Gamma)\right]^2 \tag{24}$$

where $\hat{\Omega}$ is defined as

$$\hat{\Omega} = \Omega + \varepsilon \ln\left(\hat{L}/L\right) \tag{25}$$

In equations 11, 21, and 25, $\hat{L}$ is a fixed dimension, regardless of the body being analyzed, whereas L is a characteristic dimension that scales with the body. Equation 25 ensures that equations 11, 21, and 22 will predict the correct mode mix for those cases where an oscillatory singularity exists. That is, Ω is determined for a specific crack tip element geometry and is based on the characteristic dimension L. The scaling of $\hat{\Omega}$ given by equation 25 ensures that the same Ω will predict the correct mode mix for arbitrary loadings of a geometrically similar element with different absolute dimensions. [1] When $\varepsilon \neq 0$, an oscillatory singularity is predicted, and G_I and G_{II} are dimensionally convenient generalizations of their classical definitions; the use of these parameters in crack growth problems is similar to the use of the complex stress-intensity factor. When $\varepsilon = 0$, an inverse-square root singularity is predicted and G_I and G_{II} retain their classical definitions. Also, when $\varepsilon = 0$, $\hat{\Omega} = \Omega$ (cf. equation 25) and for notational purposes, it is convenient to make this substitution in equations 23 and 24. Regardless of the value of $\hat{\Omega}$, the sum of equations 23 and 24 will always equal that given by equation 5.

If the preceding analysis is carried out in three dimensions [8] and the two cracked and one uncracked region of the element are specially orthotropic ($A_{16} = A_{26} = B_{ij} = D_{16} = D_{26} = 0$ in conventional [11] notation), then the mode III ERR, G_{III}, is obtained as [8]

$$G_{III} = \frac{c_3}{2}\left(N_c^y\right)^2 \tag{26}$$

where
$$c_3 = \frac{1}{A_{66}^1} + \frac{1}{A_{66}^2} \tag{27}$$

and
$$N_c^y = -N_6^1 + \frac{A_{66}^1}{A_{66}^u}\left(N_6^1 + N_6^2\right) \tag{28}$$

In equations 26, 27, and 28, N_c^y is the second concentrated crack tip force, which acts in the plane of N_c but perpendicular to it, that arises for three-dimensional problems. [7, 8] The superscripts 1, 2, and u in the above equations indicate that these values are for the cracked region that is above the crack, the cracked region below the crack, or the uncracked region, respectively. Also, A_{66} and N_6 are defined using their conventional definitions for in-plane shear stiffness and shear force per unit length, respectively, for a laminated plate. [11] It is pointed out

that a more general expression for G_{III} has been derived [8] where the restrictions of special orthotropy are removed. However, only the specially orthotropic case will be considered herein, and for this reason the considerably more complicated general equations are not presented.

In the preceding subsection, an assumption of a near-tip singular zone was made for mode decomposition that was not necessary for the determination of total ERR. Rather, for total ERR it need only be assumed that classical plate theory is appropriate for determining far-field stresses, strains, and strain energies. Thus, one could obtain G, and also choose to decompose it, without assuming that a singular field exists. Such a decomposition could be accomplished, for example, by choosing an $\hat{\Omega}$ that does not coincide with the singular field-based value and would partition the total ERR into non-classical mode I and mode II components. This issue is discussed below.

For those laminated composites where the assumption of a singular zone applies, $\hat{\Omega}$ may be chosen such that the crack tip element (CTE) and the classical, singular field (SF) solution coincide. A method for doing this is described in references 1 and 13 and tabulated results for $\hat{\Omega}$ for a variety of crack tip element geometries are presented in reference 1. It will be shown in sections 3 and 4 of this report that, when $\hat{\Omega}$ is chosen in this manner, the CTE predictions coincide quite closely to the finite element (FE) results for problems where inverse-square root as well as oscillatory singularities exist. Problems where the SF-based approach is valid to predict delamination growth consist of those materials, structures, and loading geometries where the length of the near-tip process zone is small compared to the radius of the singular zone. Typically, this latter radius is scaled by the smallest characteristic dimension in the problem, which for unidirectional laminates is generally the thickness of one of the cracked regions and for multidirectional laminates is generally the single ply thickness.

When the size of the process zone is *not* small compared to the smallest characteristic dimension in the problem, then the concept of a singular zone no longer applies. That is, the expressions for the near-tip stresses, strains, and displacement fields may be quite different from those given by the classical SF-based result; thus, the SF mode mix is not appropriate for these cases. It is likely that different geometries that this method predicts to be at the same mode mix will display different toughnesses. When this occurs, a different definition of mode mix is required. This definition should reflect the dependence of toughness on the remote loading in such a manner that different geometries that are predicted to be at the same mode mix display the same toughness. The concentrated crack tip moment, M_c, and shear forces, N_c and N_c^y, which are computed as part of the crack tip element analysis appear to be well-suited for this purpose. These quantities do *not* depend on the existence of a singular zone, they can be used to directly express ERR, and they are not affected by the near-tip damage state. However, the concentrated crack tip moment and shear forces have different units. Thus, if these quantities were used directly, i.e., by expressing G_c as $G_c(N_c/M_c)$, then the resulting toughness versus mode mix curve would be sensitive to changes in geometry and therefore would not be suited to characterizing crack growth in a manner that would be useful in a predictive methodology. If a dimension (such

as a single ply thickness) were introduced to nondimensionalize N_c/M_c, there is no guarantee that this ratio would provide the desired result.

A better approach, and in the same spirit, is based on equations 23 and 24 and an effective value of Ω (used here in lieu of $\hat{\Omega}$). The effective Ω provides the necessary scaling normalization for the influence of N_c/M_c and contains the solution with a singular zone as a special case. As energy release rate, equation 5, is independent of Ω and the existence of a singular zone, the key issue is whether an expression for Ω can be obtained that will account for the dependence of the toughness on the geometry of the near-tip region (layup, stacking sequence, and delamination location) and its local loading. This effective value of Ω, used with equations 23 and 24, will result in a non-classical partitioning of the total energy release rate that is implicitly based on the ratio of N_c/M_c. The implicit, rather than explicit, dependence on N_c/M_c is primarily due to a current lack of understanding of the exact physics controlling the conditions for the onset of crack advance in this type of a material. As such, at present, the effective value of Ω (or Ω-effective, as may be used subsequently) can only be obtained experimentally. A method for doing this is described and illustrated in section 5.4.2.

Finally, it is pointed out that, for those materials with small process zones, use of Ω-effective may be used to circumvent the practical problems associated with the oscillatory singularity. That is, a mode mix definition based on the singular oscillatory field is a special case of the Ω-effective approach. The $\beta=0$ approach, which has been proposed [1, 14] for materials with relatively small process zones for predicting delamination growth at interfaces where there is an oscillatory singularity, is also a special case of the Ω-effective approach. As such, the determination of an Ω-effective for use with the CTE equations is a robust methodology and can be used for general application without regards to the process zone size or the existence or nature of the singularity.

3. EXAMPLE PROBLEMS IN TWO DIMENSIONS.

3.1 INSTABILITY-RELATED DELAMINATION GROWTH.

The problem of instability-related growth of a through-width delamination may be solved analytically by using a global cylindrical buckling analysis along with a local crack tip element analysis. [15] Figure 2 shows a cross-sectional view of a laminate containing two delaminations. These delaminations are assumed to be located symmetrically with respect to the laminate's midplane, and the laminate is assumed to be midplane symmetric. The delaminated regions, defined to be the regions bounded by the delaminations and the laminate free surfaces, may or may not be symmetric about their local midplanes. The delaminations are assumed to extend through the entire width of the laminate and the laminate is assumed to be in a state of plane stress or plane strain with respect to the y coordinate direction. Note that as the base region, defined to be the portion of the laminate bounded by the two delaminations, becomes very thick, the present problem degenerates to the commonly considered thin film geometry. [16, 17] It is assumed that for all cases being considered, the delaminated regions have slenderness ratios which are large compared to that of the base region and that under applied compressive load or

displacement, local instabilities that occur in the delaminated regions are not accompanied by any associated bending or instability in the base region or global laminate.
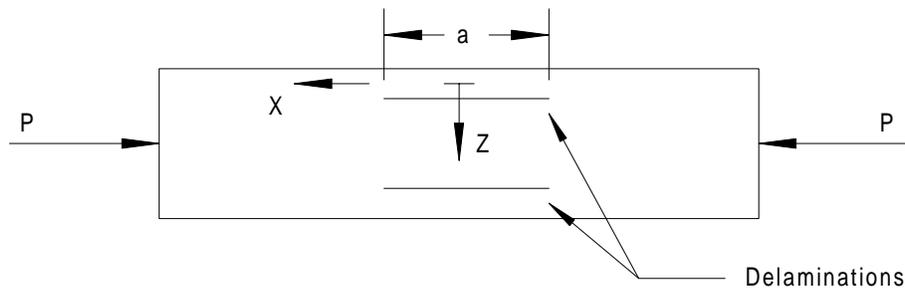
FIGURE 2. CROSS-SECTIONAL VIEW OF LAMINATE CONTAINING TWO SYMMETRICALLY LOCATED DELAMINATIONS THAT IS SUBJECTED TO COMPRESSIVE LOADING

For a specified value of globally applied load or displacement, the deformations and local force and moment resultants in the delaminated and base regions may be obtained by a cylindrical buckling analysis. [15, 17] The postbuckled laminate appears as shown in figure 3a, with all internal force and moment resultants shown in their positive conventions (the actual in-plane forces are compressive in this problem and therefore the reverse of those shown in figure 3a). The right-hand edge of the laminate of figure 3a corresponds to the center of the delamination. Thus, by symmetry, the load resultants in the delaminated and base regions, N_x^D and N_x^B respectively, act in the horizontal direction. These resultant forces, as well as the resultant moment in the delaminated region, M_x^D, and its center-point deflection, W, are given as a function of applied load or displacement by the cylindrical buckling analysis. By symmetry, the moment in the base region is zero.

FIGURE 3a. POST-BUCKLED CONFIGURATION

Figure 3b shows the crack tip element and local loading. The element is assumed to be cut from the laminate very near the crack tip. Note that minor modifications to the crack tip element formulation described in section 2 need to be made to enforce the symmetry constraints. The crack tip element analysis is linear; all nonlinearities in the problem are accounted for by 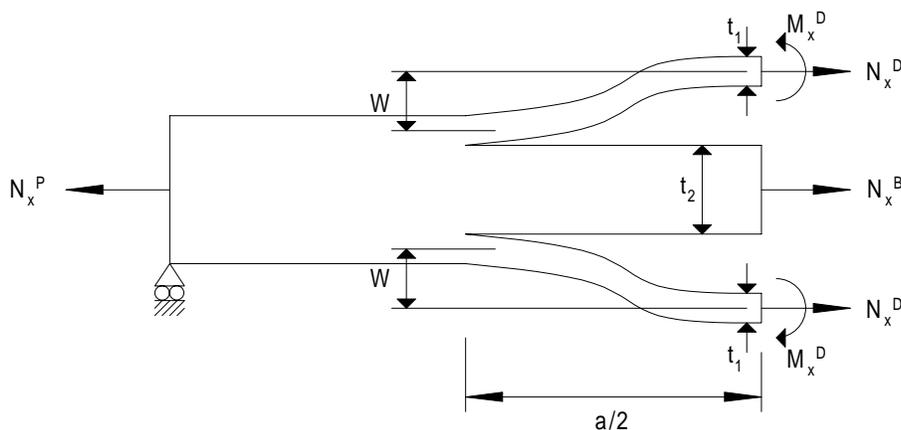the loading on the element. That is, a comparison of figures 3a and 3b indicates that the loads, N, N_1, and N_2, and moment, M_1, acting on the crack tip element are given by

$$N_1 = N_x^D \qquad N_2 = \frac{N_x^B}{2} \qquad N = N_1 + N_2 \qquad M_1 = M_x^D - N_x^D W \tag{29}$$

Substituting these loads into the crack tip element equations provides an analytical methodology for determining mixed-mode energy release rates as a function of the applied far-field loading.
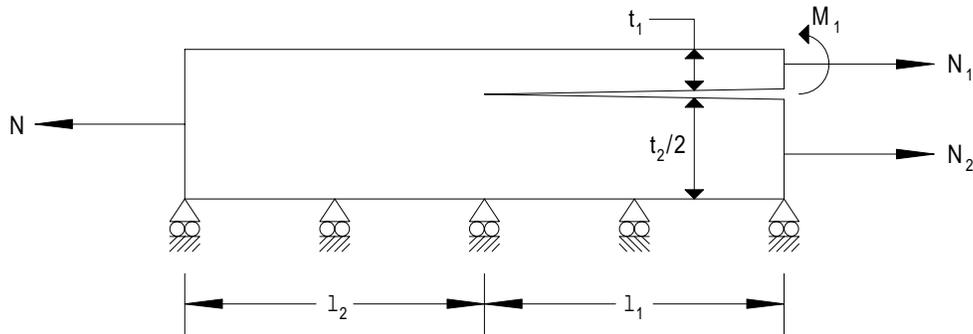
FIGURE 3b. CRACK TIP ELEMENT AND LOADING FOR DELAMINATION BUCKLING PROBLEM

Figures 4a and 4b present comparisons for total energy release rate and mode ratio between the crack tip element analysis and a geometrically nonlinear finite element analysis. [15] The geometry is a $[0_2/90/0_2]_{3s}$ graphite/epoxy laminate with delaminations at the interfaces between the 5th and 6th and 25th and 26th plies. The delamination length, a, is equal to 50.8 mm and the laminate length is 146.0 mm. The laminate is assumed to be in a state of plane strain. The horizontal axis, denoted as applied compressive strain, is the deformation of one of the loaded ends of the laminate (the center-point is assumed to be fixed with respect to in-plane deformations) divided by the laminate half-length. The value of $\hat{\Omega}$ used in the crack tip element equations was 14.6° and was found by a linear finite element analysis of the crack tip element geometry. Note that, since delamination growth occurs at a 0/0 interface, the stress singularity in this problem obeys a classical inverse-square root relation.

10

FIGURE 4a. COMPARISON OF TOTAL ERR FOR A $[0_2/90/0_2]_{3S}$ LAMINATE

FIGURE 4b. COMPARISON OF MODE RATIO FOR A $[0_2/90/0_2]_{3S}$ LAMINATE

11

Note from figures 4a and 4b that essentially the same values of energy release rate and mode ratio are predicted by the crack tip element and finite element methods. The energy release rate is seen to be predominantly mode II with the ratio G_{II}/G increasing with increasing applied compressive strain. As the applied strain continues to increase, $G_{II}/G \rightarrow 1$; this is followed by 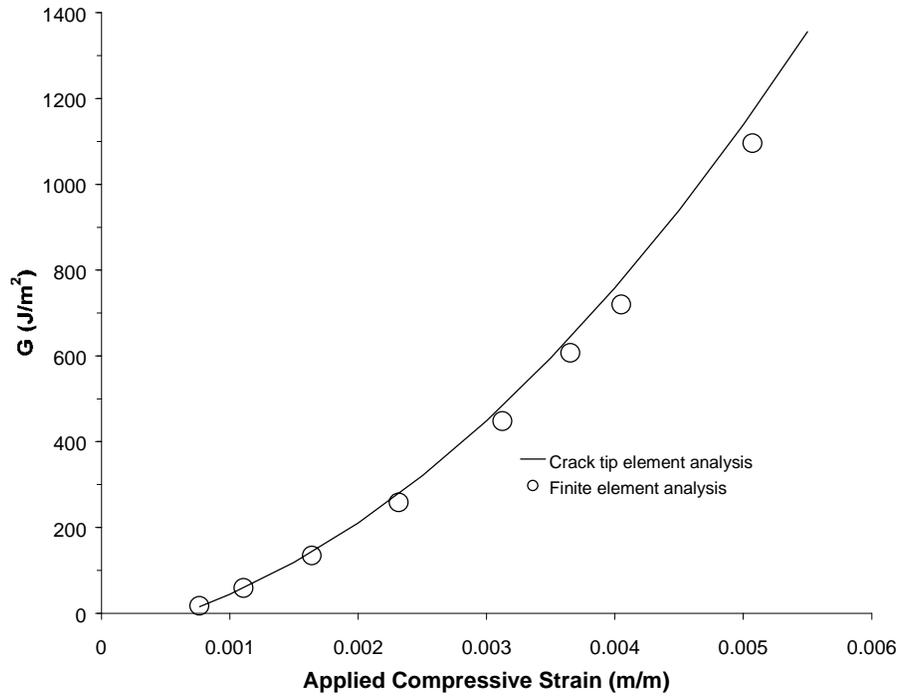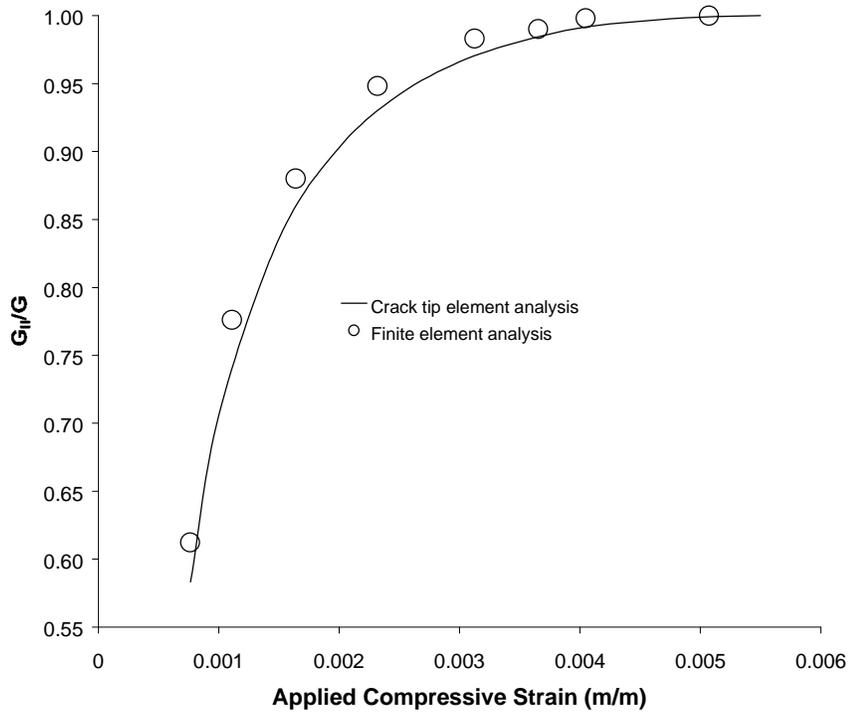crack face contact. Both the finite element and crack tip element analyses predict crack face contact to occur at the same value of applied strain (for the crack tip element analysis, this occurs when $K_I \leq 0$). To obtain energy release rates beyond this point, crack face contact constraints, along with an accounting for frictional effects, are required.

In this and other similar examples showing the correlations between crack tip element and nonlinear finite element analyses for the instability-related delamination growth problem [15], the utility of the crack tip element approach is clear. Only a single, linear finite element analysis need be performed to obtain Ω; thereafter, all results are generated analytically. For certain specific problems, no finite element analyses are required, as the value of Ω may be taken directly from reference 1. Conversely, the nonlinear finite element model contained approximately 13,600 global degrees of freedom and was extremely time-consuming to develop and run. The use of the crack tip element analysis, along with an appropriate mixed-mode delamination growth law, has been shown to accurately predict the onset of delamination growth in instability-related delamination growth experiments on honeycomb sandwich panel laminates. [18]

3.2 FREE EDGE DELAMINATION.

The problem of free edge delamination under combined in-plane, bending, and/or hygrothermal loading may also be solved using the crack tip element approach. [14, 19, and 20] Figure 5 shows a midplane symmetric laminate with a single delamination at its free edge. With reference to the figure, the term "sublaminates" is used to denote the regions bounded by the delamination and the laminate's free surfaces. It is assumed that the delamination length, a, is large compared to the thickness of either of the sublaminates. In what follows, only cases of a laminate subjected to hygrothermal loading and/or a uniform axial strain in the x_1 direction are considered. The more general case, where bending loads are included, is presented in references 19 and 20.
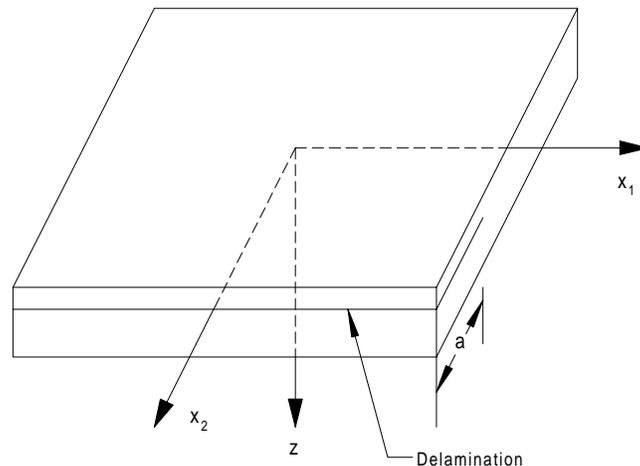

FIGURE 5. LAMINATE CONTAINING A FREE EDGE DELAMINATION

In order to obtain the local crack tip element loading, the classical laminated plate theory solution to the uncracked laminate under uniform axial strain or hygrothermal loading is first obtained. A transverse stress distribution is obtained for which the resultant transverse force, N_2, and moment, M_2, vanish along those faces of the laminate which are defined by a normal vector in the positive or negative x_2 direction. Now a crack is introduced at an arbitrary interface. In order to account for the presence of the crack, the resultant transverse forces and moments along the free edge of each of the sublaminates, as well as the shear and normal stresses along the crack plane, must now vanish. To achieve this, the solution to the problem where the sublaminates are loaded by transverse forces and moments which are equal and opposite to those which are given by the uncracked solution is superposed onto the solution to the uncracked laminate. For a single delamination, this superposition problem is the crack tip element; for symmetrically located delaminations, the superposition problem is a modified crack tip element [14, 20] which is similar to that used for the instability-related delamination growth problem. The forces and moments in the superposition problem are found by appropriate integration of the stress field from the classical laminated plate theory solution for the uncracked laminate and loading of interest. [14, 19 and 20] Since the ERR for the uncracked laminate is zero, the total ERR and mode mix are equal to those for the crack tip element superposition problem. [14, 19, and 20]

As an example, consider the determination of the energy release rate in a [45/0/-45/90]$_s$ T300/5208 laminate with delaminations at both -45/90 interfaces. The laminate is subjected to a uniform strain, $\varepsilon_o = 0.00652$, in the global x_1 direction. The value of the energy release rate for various percentage weight gains of moisture and a residual thermal stress due to a cool down of -156ºC are presented in figure 6. Also presented in figure 6 are finite element results taken from reference 21. As expected, essentially the same values are predicted. Complete details of this analysis are presented in reference 14.
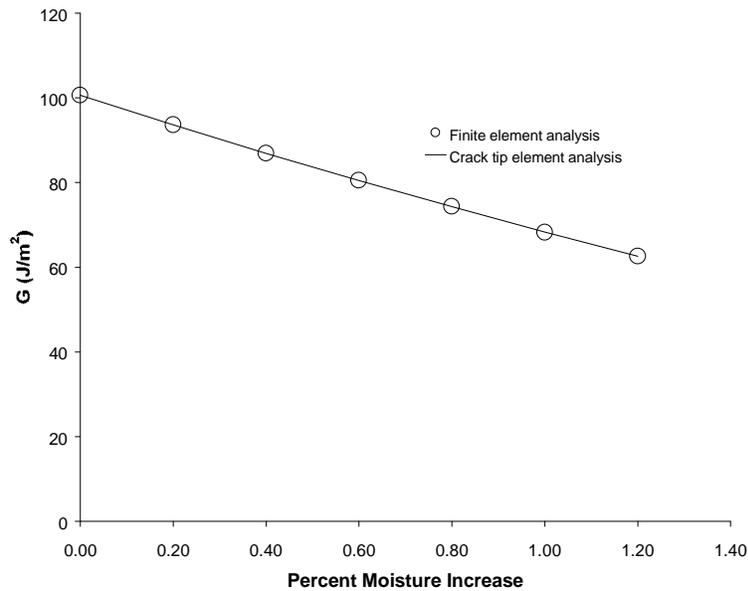

FIGURE 6. ERR VERSUS HYGROSCOPIC LOADING FOR A [45/0/-45/90]$_S$ T300/5208 LAMINATE WITH EDGE DELAMINATIONS AT BOTH -45/90 INTERFACES

Next, consider the case of edge delamination in a $[0/\pm35/90]_s$ T300/5208 laminate under mechanical, thermal, and hygroscopic loadings. Delaminations are assumed to exist at both -35/90 interfaces. Due to the dissimilar material properties above and below these interfaces, an oscillatory stress singularity exists and individual energy release rate components as found by finite element analyses are dependent upon the level of mesh refinement. [14, 22] For example, under a uniformly prescribed axial strain, the mode ratio, G_I/G, in this problem has been found to vary from 0.21 to 0.28, depending upon the size of the elements surrounding the crack tip. [22] O'Brien, et al. [21] also analyzed this laminate and reported a mode ratio of 0.265 for uniform axial extension. Other researchers [23] have also adopted this type of an approach, which can be considered the mode ratio based on a finite crack extension. This definition of mode ratio may also be adopted in the crack tip element analysis by choosing $\hat{\Omega}$ such that G_I/G under uniform axial loading equals 0.265; this correspondence is obtained using $\hat{\Omega} = 6.38°$. [14] A comparison of the crack tip element and finite element predictions for this case is presented in figure 7. These results are for the $[0/\pm35/90]_s$ laminate at a temperature of 156°C less than its stress free temperature and subjected to a uniform axial strain in the x_1 direction of $\varepsilon_o = 0.00254$. Results are presented for various levels of moisture absorption. The finite element results are taken from reference 21; excellent correlation between these values and the crack tip element predictions is observed.
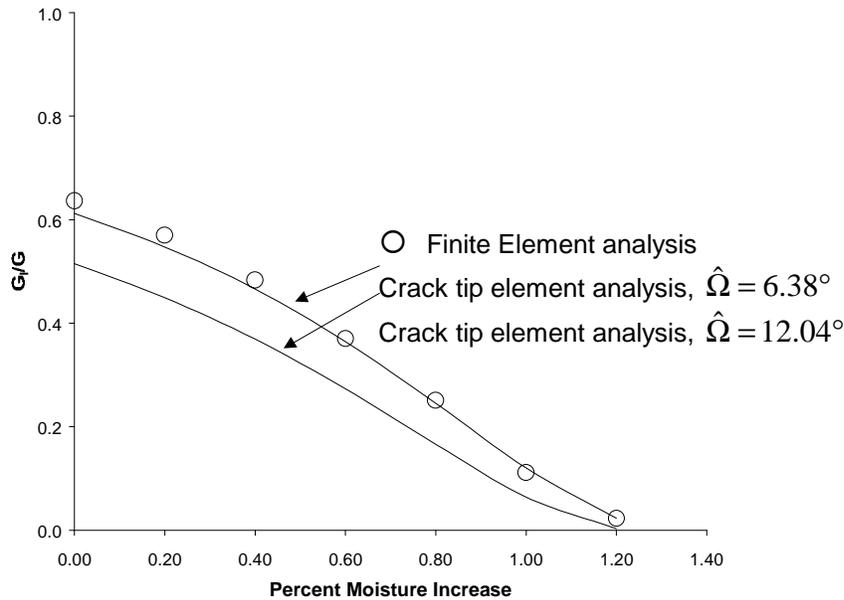
FIGURE 7. MODE RATIO VERSUS HYGROSCOPIC LOADING FOR A $[0/\pm35/90]_s$ T300/5208 LAMINATE WITH EDGE DELAMINATIONS AT BOTH -35/90 INTERFACES

Also presented in figure 7 are predictions by the crack tip element method and the β=0 approach. In the β=0 approach, one of the Poisson's ratios of one of the materials bounding the crack is changed such that β, and hence ε, equals zero (cf. equation 12). This gives an inverse-square root singularity. [1] Making this modification, one finds $\Omega = \hat{\Omega} = 12.04°$. [14] For comparison, under the case of pure axial extension (no hygrothermal loading), this problem has also been

solved by the FE method and the resin interlayer approach. In this approach, a thin resin interlayer is modeled above and below the plane of the crack. Interestingly, for pure mechanical loading, both the β=0 approach and the resin interlayer approach predict $G_I/G = 0.187$ [14]; in view of all of the results to date, identical predictions by these two approaches would also be expected for the hygrothermal loading cases. The resin interlayer approach perhaps provides the most physically appealing results; however, this approach suffers from a number of drawbacks. These include difficulty in modeling, dependence of fracture mode ratio on resin modulus and resin thickness, and a change in scale of the singular field. [24] Conversely, the β=0 approach is simple to perform, produces a unique value of mode ratio and, for all problems studied to date, produces a mode ratio that is within those obtained by the resin interlayer approach for physically realistic values of resin thickness and modulus. [24] For these reasons, the β=0 approach may be preferable for general use.

Finally, one could choose to explicitly include ε−based effects in the prediction of fracture. In this approach, one would compare the complex stress-intensity factor at a given mode mix, equations 11 and 22, to the mode mix-dependent critical value. Alternatively, the total ERR, given by equation 5, may be compared to its critical value at the appropriate phase angle, equation 22. To illustrate the accuracy of the ERR and mode mix predictions by the crack tip element approach, table 1 presents comparisons of the total ERR, G_T, and the phase angle, ψ, as obtained by FE and crack tip element analyses for the problem of figure 7 under various applied loads. For simplicity, the loading is specified in terms of M_c and N_c. The material properties used in these calculations are taken from reference 14. The phase angle is defined using $L = \hat{L} = t_1$, where t_1 is the thickness of the upper delaminated region. The FE values were obtained using the modified crack surface displacement method described in reference 1. The bimaterial constant, ε, in this problem equals 0.0361, and the mode mix parameter was found, using the technique described in reference 1, to be $\Omega = 17.51º$. Excellent correlation between the FE and crack tip element results is observed. All cases show correlations in ERR of better than 1.6% and correlations of phase angle of better than 1.7º. However, due to the large amount of experimental data that is necessary to support this approach, it is likely better to restrict this type of prediction methodology to fracture between dissimilar homogeneous materials. [1, 13]

TABLE 1. COMPARISON OF CRACK TIP ELEMENT (CTE) AND FINITE ELEMENT (FE) RESULTS FOR ERR AND MODE MIX FOR FREE EDGE DELAMINATION IN A [0/±35/90]S LAMINATE

Load Case	N_c (KN/m)	M_c (Nm/m)	FE		CTE	
			G_T (J/m^2)	ψ (deg.)	G_T(J/m^2)	ψ (deg.)
1	-17.066	0.000	69.54	-72.29	69.23	-72.33
2	-5.144	2.758	70.84	-45.97	71.07	-45.80
3	16.186	5.827	69.05	-1.99	70.12	-1.19
4	28.394	5.516	70.56	42.42	71.03	44.06
5	23.961	1.957	72.64	88.99	72.24	89.07

4. EXAMPLE PROBLEMS IN THREE DIMENSIONS.

It is well established that finite width, mode I double cantilever beam test specimens have ERR distributions such that the ERR is highest at the center of the specimen and lowest at its edges. [25] Recently, it has been shown [26] that finite width, mode II end-notched flexure specimens have ERR distributions such that the ERR is highest at the edges of the specimen and lowest at its center. Both of these effects have been shown to be caused primarily by the anticlastic curvature of the cracked and/or uncracked regions. As a result of these three-dimensional effects, mixed-mode loadings of finite width delamination toughness test specimens provide interesting cases to validate the crack tip element approach in three dimensions.

Consider a homogeneous isotropic test specimen, with Poisson's ratio equal to 0.3, subjected to the loading of figure 8. This problem was analyzed by three-dimensional FE analysis using the commercially available finite element code Abaqus Version 5.4, licensed from Hibbitt, Karlsson, and Sorensen, Inc. Twenty-noded, three-dimensional brick elements were used. The FE model had cracked and uncracked regions, a and b respectively in figure 8, that were each 256 units long. The thickness of each of the cracked regions, t_1 and t_2, was 16 units, and the width of the entire model, W, was 400 units. All elements in the model were 8 units long in the y direction; thus, the entire model contained 50 elements across its width. The mesh in the x-y plane is shown in figures 9a and 9b. The meshing technique in the x-z plane was chosen following the recommendations of reference 1 and is shown in figures 9c and 9d. The elements at the crack tip are 1 unit long by 1 unit high in the x-z plane. All of the elements in the model had length-to-width, length-to-height, and width-to-height ratios that were between 0.1 and 10.0. Two different loading cases were considered: the first was for applied end moments only ($N = 0$), and the second was for applied in-plane loads only ($M = 0$). Both the load, N, and moment, M, are defined on a per-unit-width basis following conventional plate theory notation [11] and are assumed to be distributed uniformly across the specimen's width. Total energy release rates were obtained by the virtual crack closure technique [27] generalized to three dimensions. In all cases that will be presented, ERR components that are obtained by the FE analyses are normalized by the total ERR for the specimen as obtained by a classical plate theory (CPT) analysis. In this approach, the strain energy of each of the three regions comprising the specimen are first determined by CPT, then summed, and then the resulting expression is differentiated with respect to crack area. For the loading where N=0, symmetry arguments dictate that this is a pure mode I problem, and the mode I ERR given by CPT is

$$G_I^{CPT} = \frac{12M^2}{Et_1^3} \tag{30}$$

For the loading where M=0, a CPT analysis yields

$$G_T^{CPT} = \frac{N^2}{2Et} \tag{31}$$

where G_T is defined as the total ERR (= $G_I + G_{II} + G_{III}$).
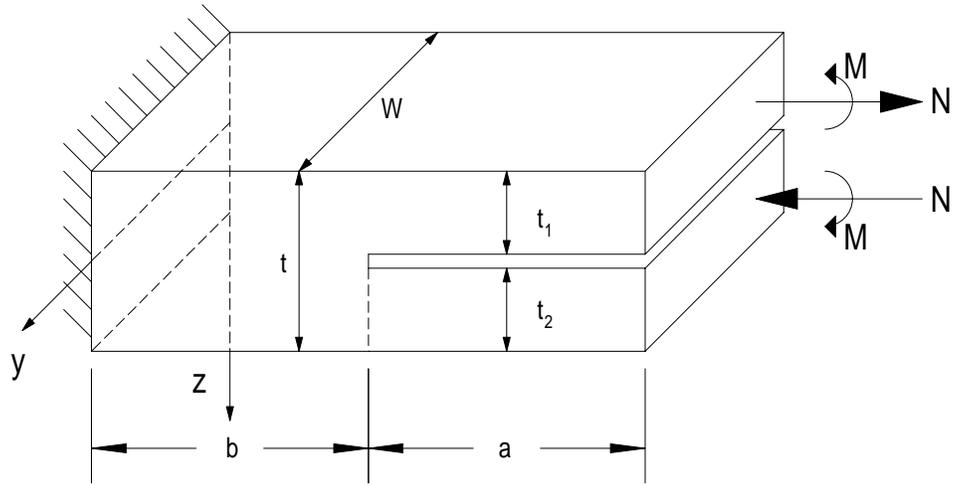
16

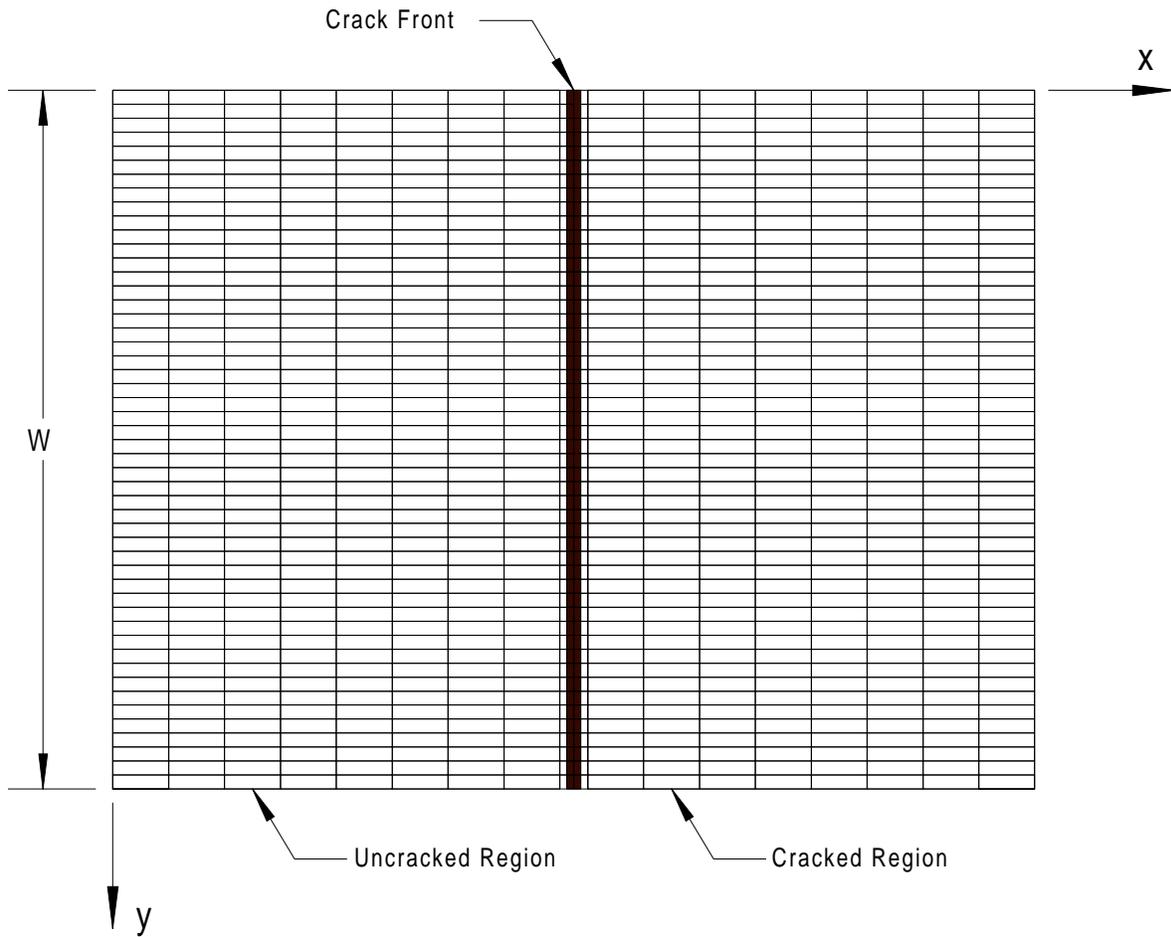FIGURE 8. THREE-DIMENSIONAL PROBLEM AND LOADING

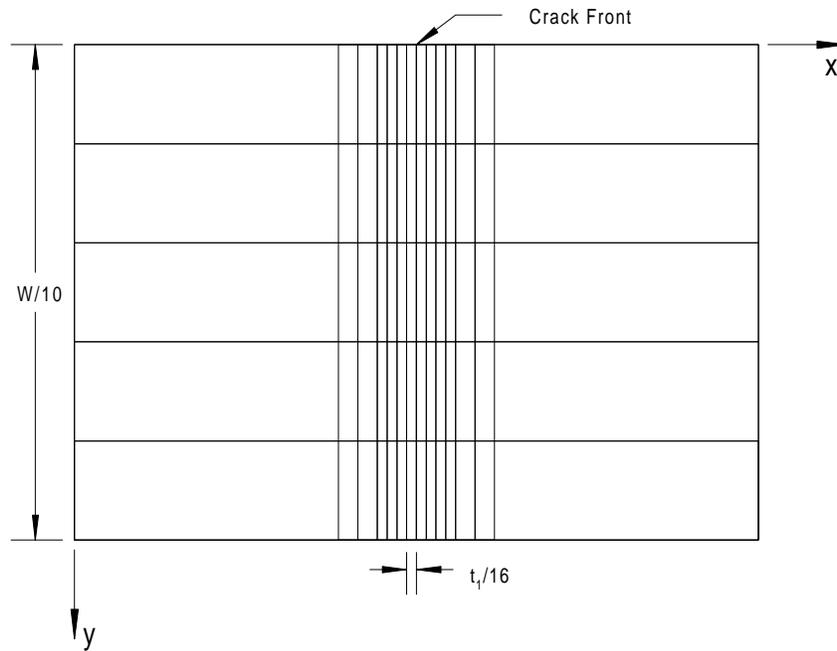FIGURE 9a. FINITE ELEMENT MESH IN THE X-Y PLANE

17

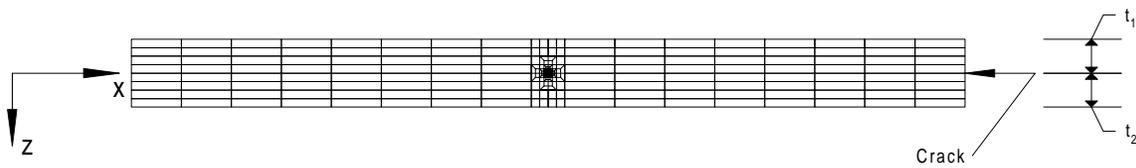FIGURE 9b. MESH IN CRACK TIP NEIGHBORHOOD IN THE X-Y PLANE

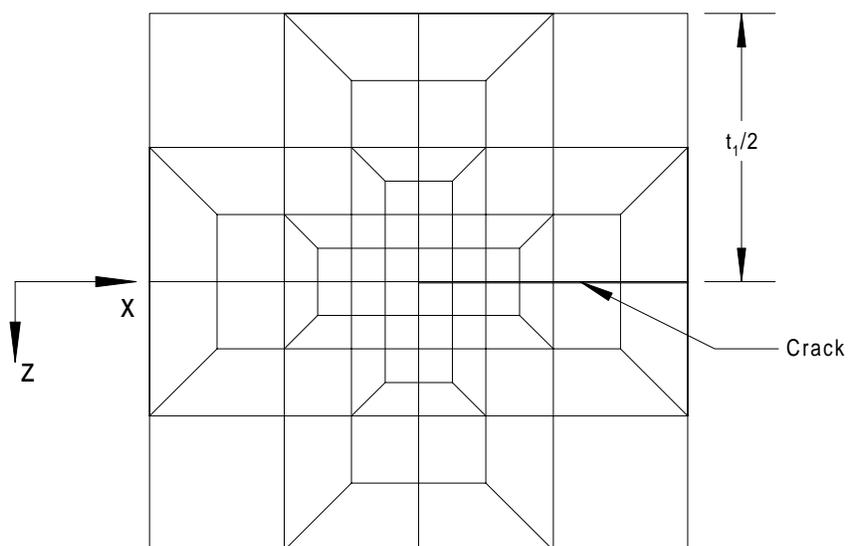FIGURE 9c. FINITE ELEMENT MESH IN THE X-Z PLANE

FIGURE 9d. MESH IN CRACK TIP NEIGHBORHOOD IN THE X-Z PLANE

18

Next, these same two problems were analyzed using the crack tip element (CTE) approach. First, a FE model was constructed of the problem utilizing nine-noded plate elements that are formulated such that the nodes are offset with respect to the midplane of the element [28]. The top portion of the specimen of interest, figure 8, was modeled using plate finite elements that are formulated such that their nodes lie along their lower surface, and the bottom portion of the specimen was modeled using elements that are formulated such that their nodes lie along their upper surface. The nodes along the crack plane, but in the uncracked portion of the specimen were constrained to have the same displacements. All of the plate theory FE models were constructed and analyzed using COMET (COmputational MEchanics Testbed program), provided by the computational mechanics branch at the National Aeronautics and Space Administration's Langley Research Center. The plan view of all COMET models looked identical to those presented in figures 9a and 9b.

The COMET models were run under the prescribed loading, and the plate theory force and moment resultants were obtained one element away (in the models used, this was one unit away or $t_1/16$) from the crack tip as a function of y. These force and moment distributions were used to obtain N_c, M_c, and N_c^y, and these results were substituted into equations 23, 24, and 26 to obtain the ERR components. Subsequently, this will be referred to as the COMET/CTE procedure.

Figure 10 presents the COMET/CTE ERR predictions in comparison to the conventional, three-dimensional, 20-noded brick FE model results for the N=0 loading. ERRs in the figure are normalized by equation 30. The specimen's width is taken to be W and therefore y/W = 0.0 and 1.0 correspond to the free edges (cf. figure 8). Note that outstanding correlation is obtained by the two methods; for a quantitative comparison, the width-averaged ERR as obtained by the COMET/CTE procedure is 0.15% greater than that obtained from the three-dimensional FE results. Here and subsequently, the term "width-averaged" is used to refer to the ERR for the entire specimen width. Since all of the elements in the model were of uniform width (8 units in y), width-averaged values are simply the average of all of the local results.
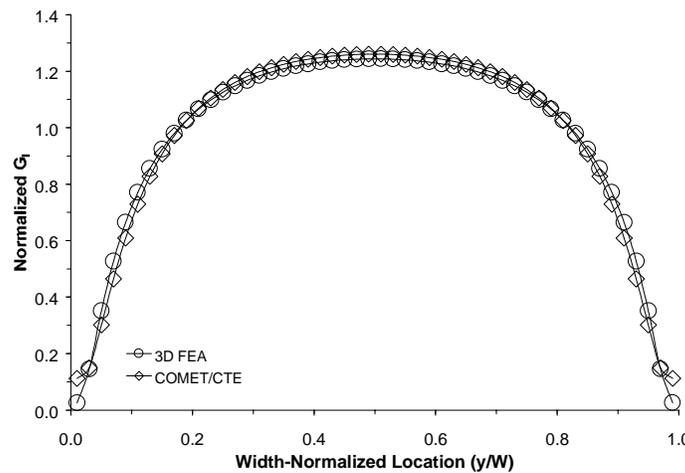

FIGURE 10. COMPARISON OF CTE AND THREE-DIMENSIONAL FE PREDICTIONS OF G_I FOR N=0 LOADING

19

Figures 11a and 11b presents comparisons of the results for the M=0 loading. ERRs in the figure are normalized by equation 31. There is no mode I component to the ERR for this loading. Figure 11a shows the mode II comparisons and evidences excellent correlation except in the regions very near the free edges where large gradients in the plate theory forces and complex three-dimensional effects are observed. In quantitative terms, the width-averaged mode II ERR as obtained by the COMET/CTE procedure is 1.40% greater than that obtained from the three-dimensional FE results. Figure 11b shows the mode III comparison. Note that the correlation between the three-dimensional FE results and the COMET/CTE results is excellent in the center of the specimen but becomes somewhat worse near the edges. These errors occur due to the large gradients in N_6 that occur in these locations. [7] In the numerical results that have been generated to date, it has been observed that the mode III ERRs as obtained by the COMET/CTE procedure exhibit errors in a boundary region that extends into the plate for approximately two uncracked plate thicknesses from a free edge. More refined COMET meshes are currently being evaluated in an effort to better capture the complex behaviors in this boundary region. However, for most practical problems of delamination, proximity to a free edge is not an issue. Overall, the accuracy of the COMET/CTE procedure for this mixed-mode problem is quite good; it was found that the width-averaged total ERR as predicted by this method was 2.58% less than that obtained from the three-dimensional finite element results.
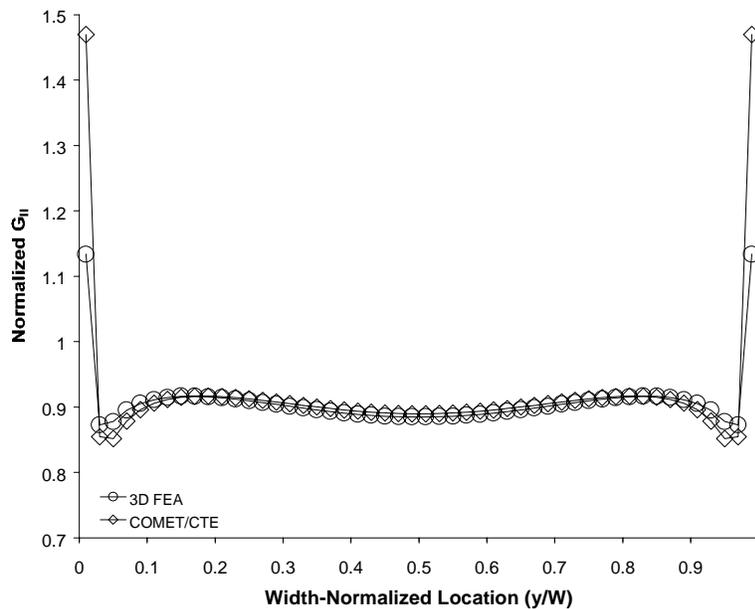

FIGURE 11a. COMPARISON OF CTE AND THREE-DIMENSIONAL FE PREDICTIONS OF G_{II} FOR M=0 LOADING
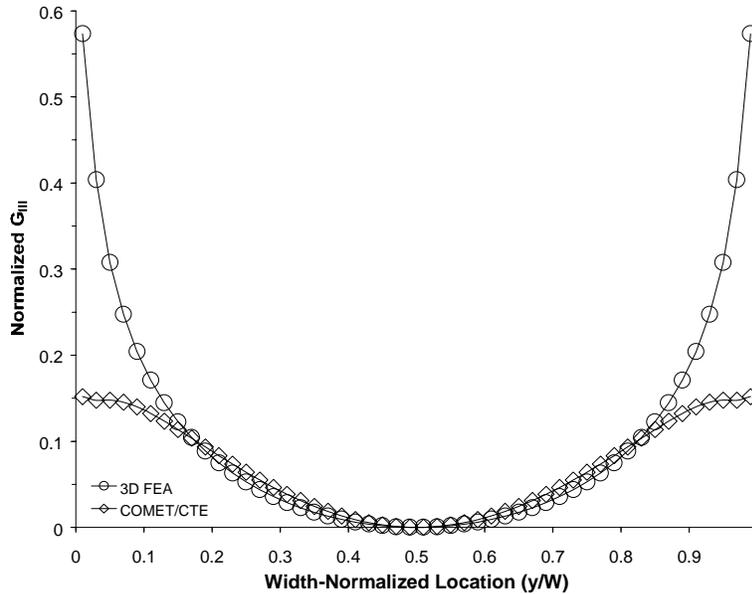
FIGURE 11b. COMPARISON OF CTE AND THREE-DIMENSIONAL FE PREDICTIONS OF G_{III} FOR M=0 LOADING

5. EXPERIMENTAL DETERMINATION OF THE DEFINITION OF MODE MIX.

In sections 3 and 4 of this report, the emphasis was on a comparison of CTE and FE results for energy release rate and mode mix in those materials and structures where a singular zone exists. However, this will not be the case for many fibrous composites. In this event, it may not be appropriate for the dependence of toughness on the loading that is evidenced by the material to be categorized in terms of the classical, singular field-based mode mix definition. In other words, use of the SF definition may produce the result that different structural geometries predicted to be at the same mode mix do not display the same toughness. When this is the case, a series of experiments must be run in order to determine the appropriate definition of mode mix for the particular material of interest. The methodology that has been developed is as follows [6, 13]:

a. Fracture tests of midplane symmetric laminates with midplane delaminations are performed. As will be discussed subsequently, all of the definitions of mode mix that are examined herein will reduce to the singular field-based definition for these geometries.

b. Fracture tests of other laminate types are performed. These data are reduced using a crack tip element analysis and various definitions of mode mix. The definition of mode mix is chosen that, when used on *all* test data, produces a physically consistent, single-valued toughness versus mode mix curve. It follows that this definition would also be used in structural analyses for that material system.

In the following subsections, brief descriptions are presented of the various test methods used. Emphasis is on mixed-mode I/II delamination. The methodology is then illustrated by application to a typical graphite/epoxy material. For completeness, the data generated as part of

21

this study are also examined using a singular field-based mode mix decomposition procedure as obtained from finite element analyses and the virtual crack closure technique. [27] The accuracy of the global mode decomposition procedure developed by Williams [29] is examined as well. Thus, when it is stated that a test geometry is analyzed by the CTE approach, it means that the mode mix, hereafter used to denote G_{II}/G, is obtained by combining equations 5 and 24 to give

$$\frac{G_{II}}{G} = \frac{\left[N_c\sqrt{c_1}\cos\Omega + M_c\sqrt{c_2}\sin(\Omega + \Gamma)\right]^2}{c_1 N_c^2 + c_2 M_c^2 + 2\sqrt{c_1 c_2}\,N_c M_c \sin\Gamma} \tag{32}$$

When it is stated that the CTE/singular field (CTE/SF) result is used, it means that equation 32 is utilized along with the singular field expression for Ω that is given in reference 1. It is pointed out here that the CTE equations do not account for the effect of transverse shear deformations on the ERR or mode mix, and therefore the CTE/SF solution will not always correspond precisely to the singular field solution as obtained by an alternative approach, such as the finite element (FE) method and the virtual crack closure technique (VCCT). Thus, in what follows, four different solutions are examined: (1) the FE result, which is likely closest to the exact singular field-based result (abbreviated as the FE/SF result); (2) the CTE/SF result; (3) the CTE/nonsingular field (CTE/NSF) result, where equation 32 is used along with an effective value of Ω; and (4) the global mode mix decomposition procedure developed by Williams. [29] For approaches (2) and (3), it is emphasized here that Ω is a function of geometry only. Thus, only one value may be used for any given specimen type (stacking sequence and delamination location). Only unidirectional laminates will be examined in the example data that is presented.

5.1 TEST METHODS USED: CENTER-DELAMINATED SPECIMENS.

In order to determine the value of Ω for the laminates with midplane delaminations, consider a double cantilever beam (DCB) test, as shown in figure 12. Any reasonable definition of mode mix would certainly consider this to be a pure mode I test. For this loading and specimen geometry, equations 8 and 9 indicate that M_c is equal to the moment in either cracked leg at the crack tip and $N_c = 0$. In order for $G_{II} = 0$, equation 32 yields $\Omega = 0$. That is, $\Omega = 0$ for any midplane symmetric laminate with a midplane delamination. [1] Thus, the first part of the experimental procedure consists of using symmetric specimens with midplane delaminations to determine the toughness versus mode mix relation. The mode mix may be obtained by FE analysis, by the CTE analysis with $\Omega = 0$, or by the analysis of Williams. [29] Small differences between the various methods will be obtained due to the different ways that transverse shear deformations are accounted for. The test methods that were used in this study are described in the following sections.
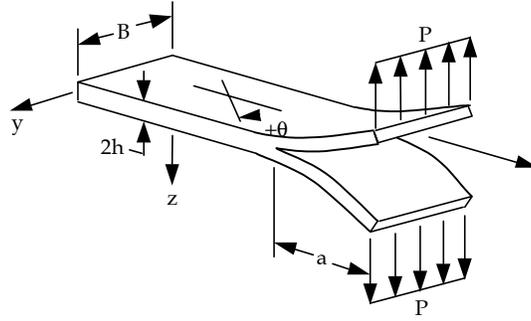
FIGURE 12. THE DOUBLE CANTILEVER BEAM TEST

5.1.1 Double Cantilever Beam Test.

Double cantilever beam tests may be used to determine the mode I fracture toughness. [30] The toughness may be found from the load and deflection data by compliance calibration by using the fundamental equation between ERR and the derivative of compliance [31]:

$$G = \frac{P^2}{2B}\frac{\partial C}{\partial a}$$ (33)

Here, B is the specimen's width, C is its compliance, and a is the crack length. Compliance as a function of crack length may be obtained for each specimen from the slope of its load versus deflection data. The method of least squares can be used to curve fit these data and to obtain the coefficients r and n in the equation

$$C = ra^n$$ (34)

Substituting equation 34 into equation 33 yields

$$G_{Ic} = \frac{nP_c\delta_c}{2Ba}$$ (35)

where P_c and δ_c are the load and deflection, respectively, at the onset of crack advance.

5.1.2 End-Notched Flexure (ENF) Test.

Figure 13 presents a drawing of the ENF test [32], which may be used for the determination of G_{IIc}. The ENF is recommended over other mode II tests, such as the end-notched cantilever beam [3, 4], because in the former case compliance calibration can be used to reduce the data. That is, it is preferable to use test methods where one does not have to make any assumptions about material properties in the reduction of data to obtain G_c (although this is unavoidable in the determination of mode mix). The procedure described in reference 33 may be used to determine the crack length, a, and half-span length, L, for the ENF tests, and data reduction may be performed by compliance calibration. Due to possible large specimen-to-specimen variations, it is recommended that a compliance versus crack length curve be developed for each specimen that is tested. [34, 35] To this end, each specimen may be loaded to approximately 50% of its

predicted fracture load at five different crack lengths. These include the crack length at which the fracture test is to be performed and two shorter and two longer lengths. The crack length may be adjusted by placing the specimen appropriately into the test fixture. At any given crack length, the compliance is obtained from the slope of a linear least squares curve fit of the deflection versus load data. Next, a compliance versus crack length curve is obtained, for each specimen, by fitting a cubic polynomial of the form

$$C = C_0 + C_1 a + C_2 a^2 + C_3 a^3 \tag{36}$$

to the compliance versus crack length data. When this approach is adopted (as opposed to using a lower order polynomial), it is important that one screens the resulting curve fits to ensure that no inflection points exist. When this occurs, it indicates that there is an error in one or more of the compliance values and compliance testing of that specimen should be repeated.
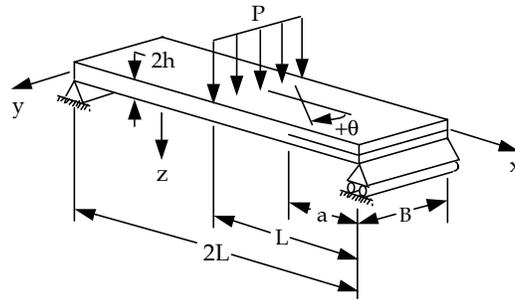
FIGURE 13. THE END-NOTCHED FLEXURE TEST

Substituting equation 36 into equation 33 and evaluating this expression at the onset of crack advance yields

$$G_{IIc} = \frac{P_c^2}{2B}(C_1 + 2C_2 a + 3C_3 a^2) \tag{37}$$

where P_c is the load at the onset of crack advance and B is the specimen's width.

5.1.3 Symmetrically Delaminated Single Leg Bending Test.

In order to use compliance calibration to reduce as much of the test data as possible, the single leg bending (SLB) test may be used to determine toughness at an intermediate mode ratio. The general SLB test is illustrated in figure 14; the term symmetric SLB (SSLB) will be used at times to distinguish the case where $t_1 = t_2$ and unsymmetric SLB (USLB) will be used at times for the case where $t_1 \neq t_2$. A finite element analysis of the SSLB geometry results in $G_{II}/G \approx 0.4$; the exact result depends on the material properties and the test geometry (L/a and a/t). [36, 37] A CTE analysis or application of Williams' mode decomposition procedure [29] yields $G_{II}/G = 0.43$. Toughness values for the SSLB test are obtained by compliance calibration in an identical manner to that used for the ENF test.

24
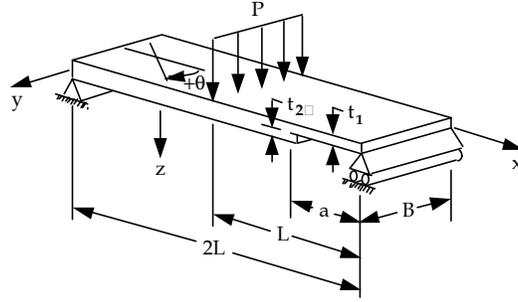
FIGURE 14. THE SINGLE LEG BENDING TEST

5.1.4 Mixed-Mode Bending Test.

The mixed-mode bending (MMB) test [38, 39], figure 15, may be used to determine the toughness of the symmetrically delaminated specimens at additional mode ratios. The procedure, described more completely in reference 40, is to use the MMB to test at mode ratios, G_{II}/G, approximately equal to 0.2, 0.4, 0.6, 0.8, 1.0. Depending on the shape of the G_c versus G_{II}/G curve, it may also be desirable to perform MMB tests at a mode ratio of approximately 0.9. An extensive study evaluating the accuracy of data reduction methods for the MMB test [40] has found that the singular field expressions for ERR and mode mix are most accurately extracted from the test data using the expressions:

$$G = \frac{16RP_I^2(a + \chi h)^2 + (R - 2)P_{II}^2(a + 0.42\chi h)^2}{16B^2D} \tag{38}$$

$$\frac{G_{II}}{G} = \frac{(R - 2)P_{II}^2(a + 0.42\chi h)^2}{16RP_I^2(a + \chi h)^2 + (R - 2)P_{II}^2(a + 0.42\chi h)^2} \tag{39}$$
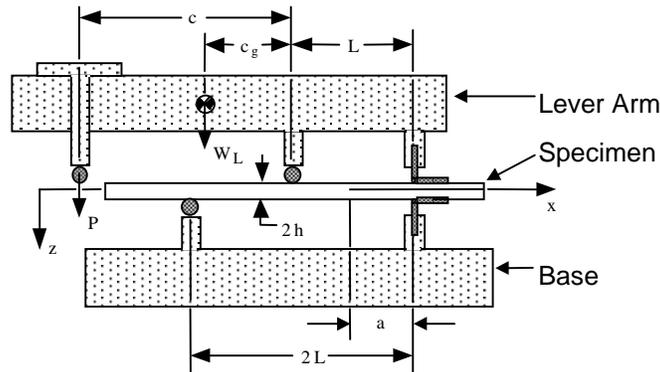
FIGURE 15. THE MIXED-MODE BENDING TEST

In equations 38 and 39, B is the specimen's width and h is the half-thickness as defined in figure 15. Also, D is the bending rigidity of the uncracked region, and R is the ratio of the bending

25

rigidity of the uncracked region to that of the cracked region. Details on the determination of D and R are presented in reference 40. P_I and P_{II} are the mode I and mode II components of the total applied load, P, and are obtained following the original superposition analysis of Reeder and Crews. [38] They are given by

$$P_I = \frac{P(3c - L) + W_L(3c_g - L)}{4L} \qquad P_{II} = \frac{P(c + L) + W_L(c_g + L)}{L}$$

(40)

where W_L is the weight of the lever arm and all dimensions are as specified in figure 15. The correction factor, χ, used to obtain an effective crack length in equations 38 and 39 is defined as

$$\chi = \sqrt{\frac{E_{11}^f}{11G_{13}}\left[3 - 2\left(\frac{\Phi}{1 + \Phi}\right)^2\right]^{\frac{1}{2}}} \qquad \Phi = 1.18\frac{\sqrt{E_{11}^f E_{33}}}{G_{13}}$$

(41)

where E_{11}^f is the flexural modulus in the x direction, E_{33} is the Young's modulus in the z direction, and G_{13} is the shear modulus in the x-z plane. Finally, if the CTE analysis or Williams' analysis is utilized to obtain the mode mix, one obtains

$$\frac{G_{II}}{G} = \frac{3P_{II}^2}{64P_I^2 + 3P_{II}^2}$$

(42)

5.2 TEST METHODS USED: SPECIMENS WITH OFFSET DELAMINATIONS.

5.2.1 Unsymmetric Single Leg Bending Test.

The USLB tests may be performed in the same manner as the SSLB tests. The only additional consideration is that, for specimens where the upper cracked region becomes thin, geometric nonlinearities may occur and invalidate the use of a compliance calibration (CC) procedure of data reduction. To this end, one can make two checks to ensure that the CC method of data reduction is valid. The first check is that the load versus deflection plot from the fracture test itself is linear to fracture. To explain the second check, consider that the tests are run in displacement control. Thus, CC simulates the growth of a crack at fixed displacement. Therefore, it is necessary that, at all crack lengths where CC is performed, the load versus deflection response of the specimen is linear up to the critical displacement. For the crack lengths shorter than that at which fracture occurs, this condition is ensured by the linearity of the fracture test itself. For the longer crack lengths, linearity may be verified after the specimen has fractured. This is done by placing the fractured specimen back in the fixture, adjusting it to the proper crack length, and then performing a compliance test to that specimen's critical displacement. Generally, this need be done only for the first specimen tested and only for the longest crack length used during CC. If the result is satisfactory, other specimens may be tested in this same geometry; otherwise, a new test geometry is chosen and the process repeated.

For illustration, figure 16 presents a graph of mode mix versus thickness ratio for the SLB test using various definitions of mode mix. The material properties of C12K/R6376 graphite/epoxy presented in table 2 were used for this figure, but little change is observed if the properties for

other typical graphite/epoxy materials are used. The FE results were obtained using the commercially available code Abaqus, licensed from Hibbitt, Karlsson, and Sorensen, Inc. The finite element models were similar to those described in references 1 and 37. For this figure, it was assumed that L = 2a (cf. figure 14) and a/t = 6.94, where $t = t_1 + t_2$. For the CTE/SF results, the expression for Ω given in reference 1 was used (the graph of Ω versus thickness ratio that will result in the singular field solution is presented in figure 23). The slight differences between the CTE and the FE results are due to the effects of transverse shear deformations on the ERR. Predictions for mode mix by Williams' approach are also displayed. This figure illustrates that predictions of mode mix by this latter approach can be quite different from the SF solution.
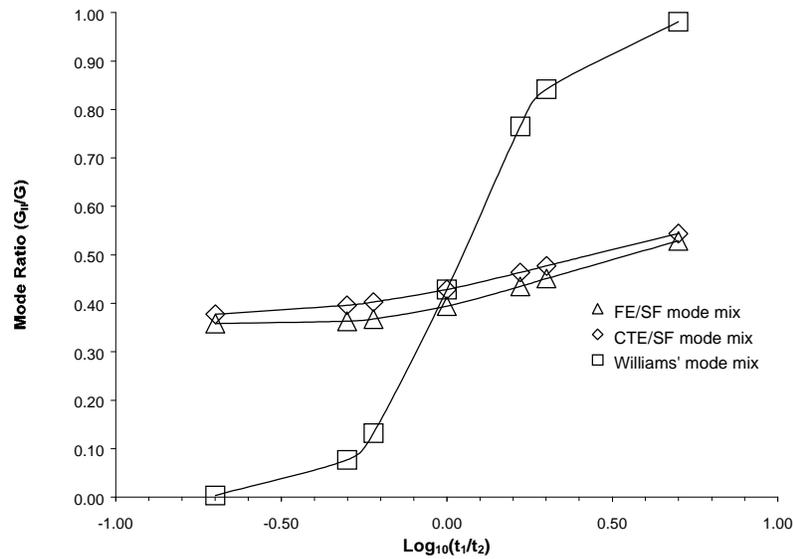
FIGURE 16. MODE MIX VERSUS THICKNESS RATIO FOR THE SLB TEST,
L = 2a, a/t = 6.94

TABLE 2. UNIDIRECTIONAL MATERIAL PROPERTIES FOR C12K/R6376
GRAPHITE/EPOXY

$E_{xx} = 146.86$ GPa	$E_{yy} = 10.62$ GPa	$\nu_{xy} = 0.33$	$G_{xy} = 5.45$ GPa
	Single ply thickness: 1.46×10^{-4} m		

As discussed in references 36 and 37, there is a slight dependence of specimen geometry (a/L and a/t, in addition to t_1/t_2) on the FE predictions for mode mix in the SLB test. Thus, in order to obtain the FE/SF mode mix for use with the test data that is presented, FE analyses were performed for the precise specimen geometries that were tested.

27

5.2.2 Unsymmetric End-Notched Flexure (UENF) Test.

The unsymmetric end-notched flexure test was proposed by Davidson and studied by Sundararaman and Davidson [37] to evaluate the fracture toughness of bimaterial interfaces. However, this test may also be used for laminated composites. The UENF test is shown in figure 17. Figure 18 presents a schematic representation of the deformation of a homogeneous UENF specimen. Figure 18(a) illustrates the cross-sectional deformations that would occur in the upper and lower materials if the crack were to exist along the entire length of the specimen. These same cross-sectional deformations are those that would be predicted if the specimen were analyzed using a classical plate theory (CPT) approach. From the relative rotations pictured in figure 18(a), it is observed that in the physical problem, the leg with the larger bending rigidity will primarily control the shape of the specimen's cross-sectional plane at the crack tip. This is illustrated in the deformed shape shown in figure 18(b). Due to the physical material continuity requirements in the problem, note that the slope of the thinner leg at the crack tip will be less than would be predicted by a CPT analysis. This also implies that the percentage of the reaction force that is carried by the lower cracked region in the figure will be greater than a CPT prediction would indicate.   Further, for a homogeneous UENF specimen, the above considerations indicate that a thicker leg on the bottom will result in crack face contact over the majority of the crack length. Thus, for all geometries, it is expected that a CPT analysis will not yield highly accurate results and, for homogeneous UENF specimens where the lower cracked region is the thicker of the two, an analysis enforcing the contact condition over much or all of the cracked interface would be required for the prediction of deformation, ERR, and mode mix. Thus, only geometries where the thicker leg is on top (cf. figure 17) will be considered here. In these cases, crack face contact occurs only in the vicinity of the right side support.
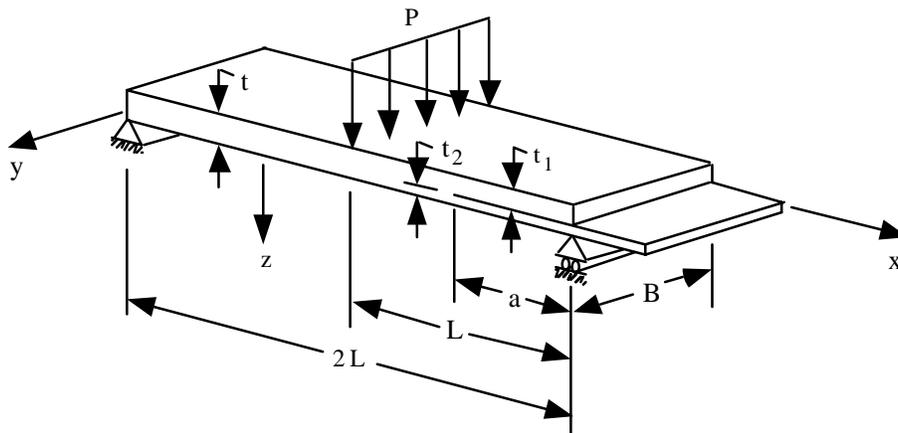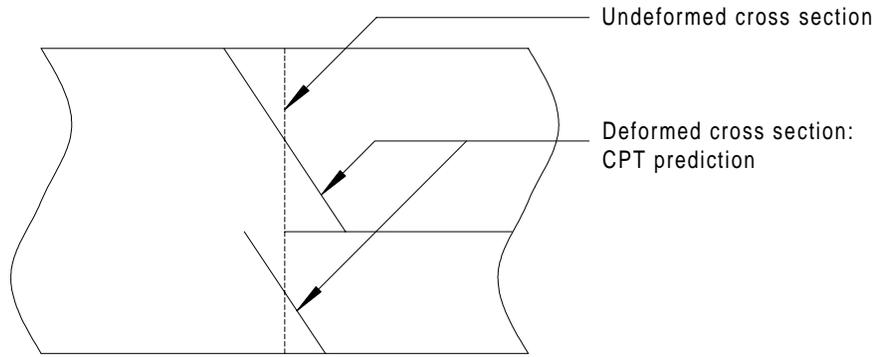

FIGURE 17. THE UNSYMMETRIC END-NOTCHED FLEXURE TEST

(a)
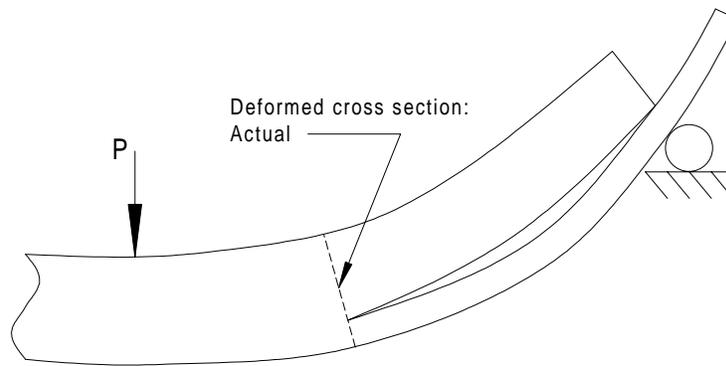
(b)

FIGURE 18. DEFORMATION OF A UENF SPECIMEN: (a) CLASSICAL PLATE THEORY
PREDICTION, (b) ACTUAL DEFORMATION

For the test data that is presented, the mode mix of the UENF test was first obtained by FE analysis. This was also done using the Abaqus FE package. All UENF geometries were analyzed using contact constraints between the two cracked regions in the region of the end support. To obtain FE predictions for mode mix, the virtual crack closure technique was used. To obtain predictions for the mode mix using the CTE and Williams' approaches, the moments in the cracked regions at the crack tip were first obtained from the finite element output. To this end, the load transferred into the top leg through each contact node was multiplied by that node's distance to the crack tip to obtain the total moment at the crack tip in the top leg, defined here as M_1 (cf. figure 1). The moment at the crack tip in the bottom leg, M_2, was obtained from static equilibrium considerations. These two moments were then used in the CTE and Williams' mode mix decomposition procedures. For illustration, typical results for the moment ratio, M_1/M_2, are presented in figure 19a; these results were generated using the material properties for C12K/R6376 presented in table 2 and all geometries were such that $L = 2a$ and $a/t = 6.94$. For reference, predictions by CPT, where $M_1/M_2 = (t_1/t_2)^3$, are also included. As indicated above, CPT underpredicts M_2 for $t_1/t_2 > 1$ and, as would be expected, the CPT solution becomes worse

with increasing $\log(t_1/t_2)$. Figure 19a clearly illustrates why the FE, rather than CPT, results for M_1 and M_2 should be used for this test.
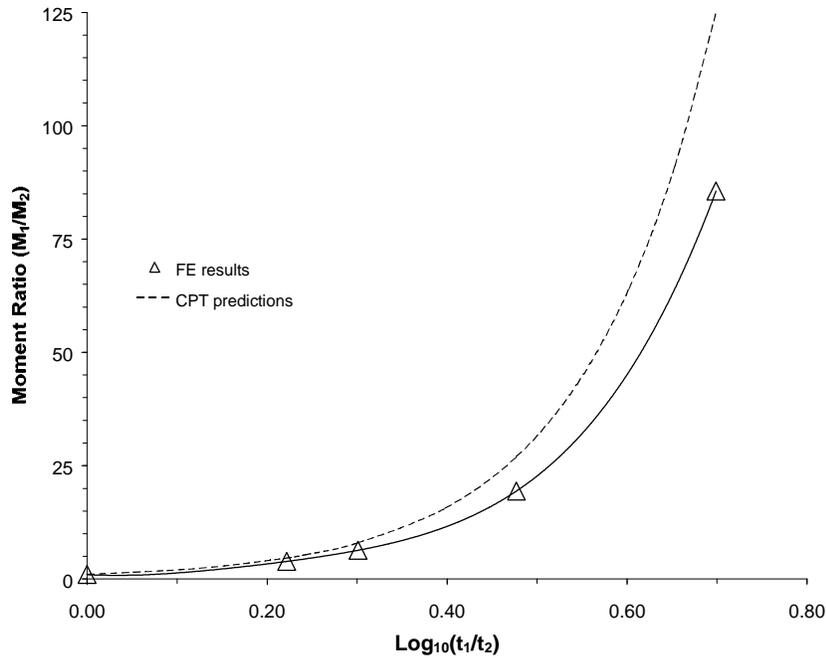
FIGURE 19a. MOMENT RATIO VERSUS THICKNESS RATIO FOR THE UENF TEST,
L = 2a, a/t = 6.94

Figure 19b presents the predictions for mode mix by the FE/SF, CTE/SF, and Williams' approaches for the geometries that were considered in figure 19a. It is observed that the FE/SF and the CTE/SF predictions are quite close; the difference is due to the effect of transverse shear deformations. As a result of the similar curvatures of the two legs, Williams' approach predicts the mode mix for all test geometries to be greater than or equal to 99% mode II. Similar to figure 16, figure 19b illustrates that predictions of mode mix by Williams' approach can be quite different from the SF solution.

As in the case of the SLB, there is a dependence of predicted results on material properties when the FE method is used, and the results of figures 19a and 19b will be slightly different if a different graphite/epoxy material is used. There is also a dependence of moment ratio and mode mix on the specimen and test geometry. Thus, for the reduction of the test data, the exact crack length, half-span length (L), thickness, and thickness ratio of each UENF specimen tested were used in the FE and other associated analyses.
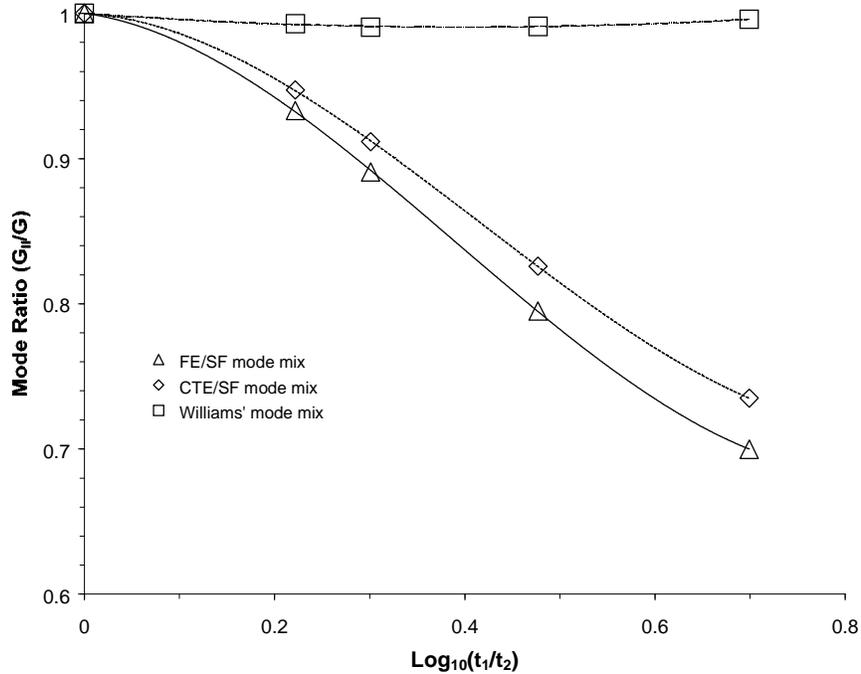
FIGURE 19b. MODE MIX VERSUS THICKNESS RATIO FOR THE UENF TEST,
L = 2a, a/t = 6.94

The compliance calibration procedure is also used to obtain the total ERR for the UENF tests. However, a modification to the procedure used for the ENF and SLB tests is required. The first compliance test is performed at the longest crack length with the upper leg of the specimen trimmed such that it ends just above the right side support, as shown in figures 17 and 18. Each time the crack length is shortened (by repositioning the specimen in the fixture), the top leg is trimmed again so that it always ends just above the support point. This step is required so that the CC procedure accurately simulates the mode of crack advance. If the top leg is *not* trimmed, then crack face contact outside of the end support will affect the load transfer between the specimen legs and accurate results will not be obtained (cf. figure 18(b)). Thus, the fracture test is performed at the shortest crack length that was used for CC. To minimize the possibility of error in the CC process, each compliance test may be performed twice. Between these two tests, the specimen should physically be removed from the fixture and then repositioned into place. The average of these two test results is used in the reduction of the test data. Finally, the compliance versus crack length data is fit with a polynomial of the form

$$C = C_0 + C_3 a^3 \qquad\qquad (43)$$

A sensitivity study [40] indicated that, when evaluating the derivative of the compliance versus crack length curve at the end of the curve, i.e., at the smallest crack length (as must be done for the UENF test), equation 43 produced results that were more accurate than those obtained using equation 36. Conversely, when evaluating $\partial C/\partial a$ at the median crack length, equation 36 is preferable. [34] All CC tests are performed to approximately 50% of the predicted critical load.

31

To ensure that CC is valid, the same two linearity checks are performed for this test as are done for the SLB.

5.3 TEST SPECIMENS, TEST GEOMETRIES, AND TEST MATRIX.

In this test program, the C12K/R6376 graphite/epoxy material system was used. The C12K fibers are similar to HTA, which is commonly used with the R6376 resin for aerospace applications, and the resin is a homogeneous, single-phase, thermoplastic-toughened system. Material and geometric properties for this system are presented in table 2. Only unidirectional, $[0]_T$ laminates were considered. All laminates were fabricated with a 12.7-μm-thick teflon sheet at the appropriate location to serve as a starter crack. No precracking was performed; that is, all crack advance data were taken directly from the preimplanted teflon starter crack. All specimens were approximately 25 mm wide.

The matrix of tests that were performed is presented in table 3. The specific test geometries were chosen to (1) eliminate any geometric nonlinearities—this was done by keeping the span lengths and crack lengths as short as possible but still several times the laminate thickness and (2) eliminate any effect of transverse compression stresses near the center roller on the perceived toughness. This latter issue was addressed by keeping the distance between the crack tip and the center roller, at the critical crack length, greater than six specimen thicknesses.

TABLE 3. TEST GEOMETRIES

Test	N_1/N_2*	FE/SF Mode Mix (G_{II}/G)†	Half-Span Length L (mm)	Crack Lengths Used for CC (mm)	Crack Length at Fracture (mm)
DCB	16/16	0.00	----	††††	57.5
SSLB	16/16	0.40	63.5	21.6, 26.7, 31.8, 36.8, 41.9	31.8
ENF	16/16	1.00	63.5	21.6, 26.7, 31.8, 36.8, 41.9	31.8
MMB	12/12	****	50.8	----	25.4
USLB	08/24	0.34	50.8	8.9, 12.7, 16.5, 20.3, 24.1	16.5
USLB	12/20	0.36	50.8	11.4, 16.5, 21.6, 26.7, 31.8	21.6
USLB	20/12	0.43	63.5	21.6, 26.7, 31.8, 36.8, 41.9	31.8
USLB	24/08	0.49	63.5	21.6, 26.7, 31.8, 36.8, 41.9	31.8
UENF	25/05	0.72	63.5	27.9, 31.8, 35.6, 39.4, 43.2	27.9
UENF	20/10	0.89	63.5	27.4, 31.2, 35.1, 38.9, 42.7	27.4
UENF	20/12	0.93	63.5	30.5, 34.3, 38.1, 41.9, 45.7	30.5

    *   Number of plies in leg 1/number of plies in leg 2.
    †   Using actual t_1/t_2 from test specimens (may vary slightly from the nominal result using N_1/N_2).
  †††† Crack advanced sufficiently to take approximately 10 data readings.
  **** 0.20, 0.40, 0.60, 0.80, 0.91, and 1.00.

5.4.1 Specimens With Midplane Delaminations.

The experimentally determined toughness versus mode mix curve for the C12K/R6376 material is shown in figure 20. A minimum of five specimens were tested in each configuration. The discrete symbols show the mean of the data and the error bars at each data point represent a spread of ±1 normal standard deviation. The critical ERRs were obtained by CC for the DCB, SSLB and ENF data, and from equation 38 for the MMB data. A number of different mode decomposition procedures are presented in figure 20. The circular symbols are used for the DCB, SSLB and ENF, and are at the mode mixities predicted by FE analyses. For the MMB, square symbols are used and are at mode mixities given by equation 39; as shown in reference 40, this result is believed to be the closest to the exact SF value. The diamonds show all of the above data when re-interpreted with Williams' approach or with the CTE/SF analysis (i.e., these two methods predict the same mode mix). For the CTE/SF analysis, this means using equation 32 and $\Omega = 0$, and for the MMB, this reduces to equation 42. The slight difference in mode mix predicted by Williams' and the CTE methods, as compared to the other results, is due to the fact that transverse shear deformations are ignored in the two closed-form approaches.
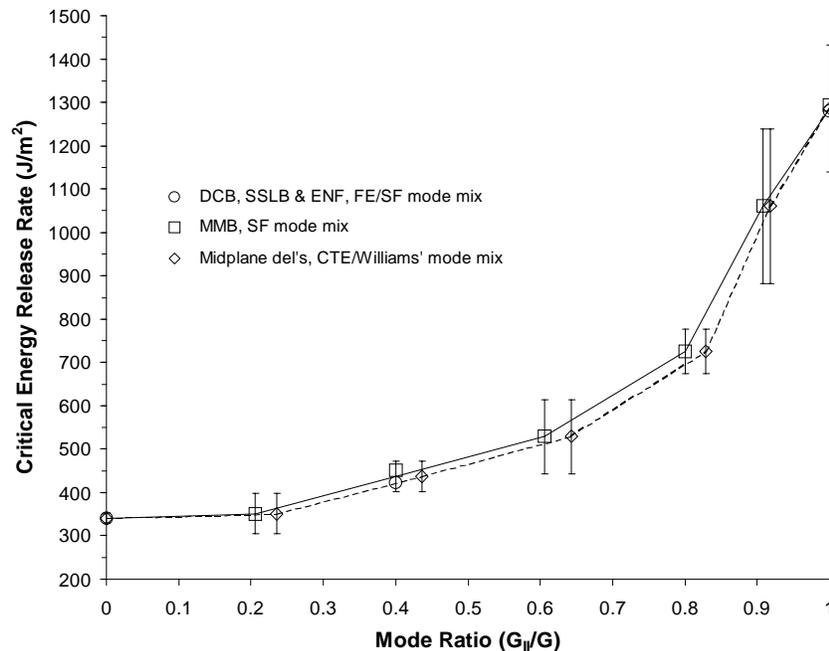
FIGURE 20. G_C VERSUS G_{II}/G AS OBTAINED FROM SPECIMENS WITH MIDPLANE DELAMINATIONS

It is pointed out here that the SLB/SF and the MMB/SF results at $G_{II}/G = 0.4$ that are presented in the figure have been kept separate to show the good correlation between the SLB and MMB test results. [40] This indicates that either one of these test methods are acceptable. However, it has been recommended that both SLB and MMB at $G_{II}/G = 0.4$ tests be run to verify the data reduction technique for MMB. [40]   The data sets from the ENF/SF and MMB/SF tests at

$G_{II}/G = 1.0$ have also been kept separate. However, the mean value from the pooled data is used for displaying the CTE and Williams' results, and the data is pooled at all locations to determine standard deviations. The standard deviations as given by the various data sets examined individually are in fact quite close, and a detailed comparison is presented in reference 40. All lines in the figure are simply a series of straight segments connecting the various mean results. For all results in figures 20, 21, and 22, the peak load observed in the test was used in the reduction of data.

5.4.2 Specimens With Offset Delaminations.

Following the development of figure 20, the offset delamination tests of table 3 were performed. At least five specimens were tested in each of these configurations. The data from these tests were reduced in three different ways: (1) FE/SF mode mix; (2) CTE/NSF mode mix; and (3) Williams' mode mix. The CTE/SF mode mix is omitted for clarity; this approach does not give significantly different results from the FE/SF approach (cf. figures 16 and 19b). In all cases, G_c was obtained by CC as described in sections 5.1 and 5.2. Thus, only the mode mix is affected by the various data reduction procedures.

Figure 21 presents the data from the specimens with offset delaminations with mode mix determined by the FE/SF approach and by Williams' approach. For reference, the results of figure 20 are also presented; the discrete data points presented in figure 20 have been omitted for clarity, but the standard deviation data have been retained. Note that neither the singular field mode mix decomposition nor Williams' approach will result in accurate predictions of delamination growth for this material. In fact, if one were to use the data of figure 20 and either of these approaches to predict delamination growth, in many cases extremely large errors would be observed.
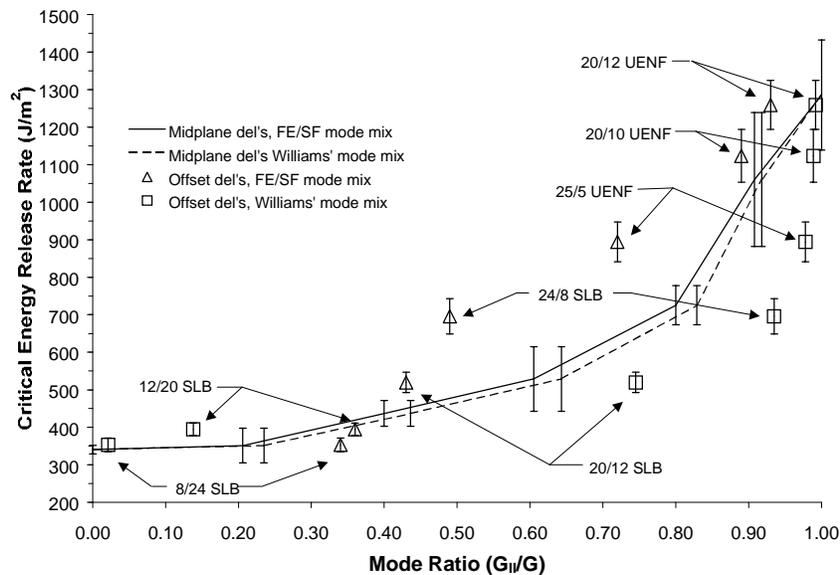

FIGURE 21. COMPARISON OF RESULTS: LAMINATES WITH MIDPLANE AND OFFSET DELAMINATIONS. Data reduction by the FE/SF and Williams methods.

Figure 22 presents the data from the offset delaminations with mode mix determined by the crack tip element/nonsingular field (CTE/NSF) approach. For reference, the CTE mode mix results of figure 20 are also presented. To facilitate the presentation, the results taken from figure 20 have been displayed by presenting the lines that follow the mean and the standard deviation values of the data. It is also pointed out here that when $t_1 = t_2$, i.e., for the case of midplane delaminations, the CTE/NSF and the CTE/SF approach are equivalent, as $\Omega = 0$ for both cases (for this reason, the distinction between CTE/SF and CTE/NSF mode mix for the midplane delaminated laminates is unnecessary). For the reduction of data from the tests of the laminates with the offset delaminations, an effective Ω has been used in figure 22.
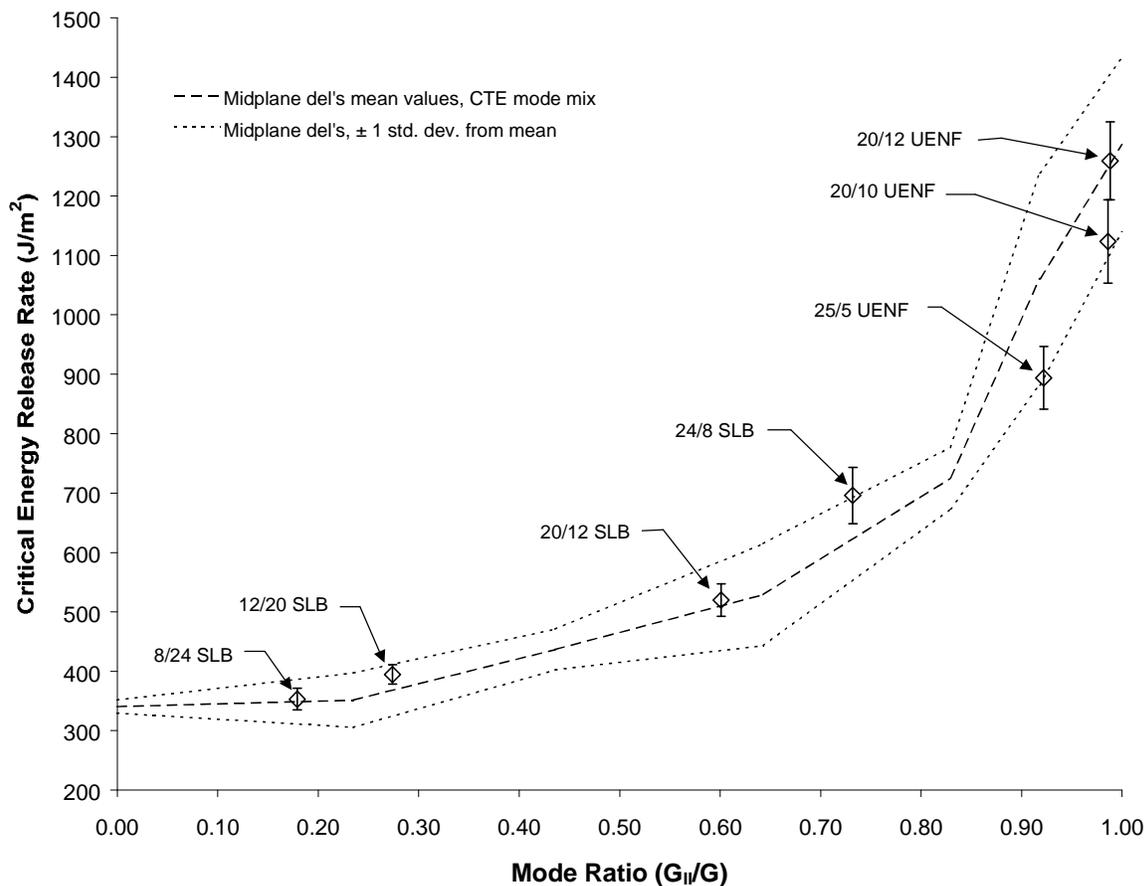
FIGURE 22. COMPARISON OF RESULTS: LAMINATES WITH MIDPLANE AND OFFSET DELAMINATIONS. Data reduction by the CTE/NSF method.

Note from figure 22 that if a CTE/NSF analysis is used to interpret all of the data, then, allowing for experimental scatter, toughness is found to be a single-valued function of mode mix. That is, this analysis is found to successfully collapse the data from the various tests. Figure 23 presents the effective Ω as a function of thickness ratio that was used in the development of figure 22. For reference, the singular field-based result, taken from reference 1, is also included. The effective Ω was obtained by enforcing the physical constraints [1] that it is an odd function of

log(t_2/t_1), that it has a limiting value that is less than approximately 30º, and that it does not contain an inflection point for $t_2/t_1 > 1$. Within these constraints, the test data was used to calculate the expression for Ω such that the same toughness was obtained from different geometries at the same mode mix. It is emphasized that the use of an effective Ω is not simply a curve fit of the data. Rather, this approach implicitly bases mode mix on the ratio of the concentrated crack tip quantities N_c and M_c, and the necessary scaling normalization is accomplished through the use of Ω-effective. Toughness versus mode mix results are then easily expressed in terms of the nonclassical definitions of the ERR components, as has been done in figure 22. It is interesting that the limiting value of Ω-effective is fairly close to the singular field-based result, and that the primary difference is a more rapid rise in Ω-effective with thickness ratio to its limiting value. Structural analyses may now be performed with the CTE analysis, the effective Ω of figure 23 and the failure locus of figure 22. This approach assumes that crack advance will occur when G, at that particular NSF mode mix, reaches its critical value, G_c. The NSF mode mix definition accounts for the effect of the geometry and loading on toughness in the same manner that the classical approach will in materials that have small-scale process zones, and accurate crack growth predictions will be obtained. Note that this also obviates the need for local FE analyses to obtain mode mix.
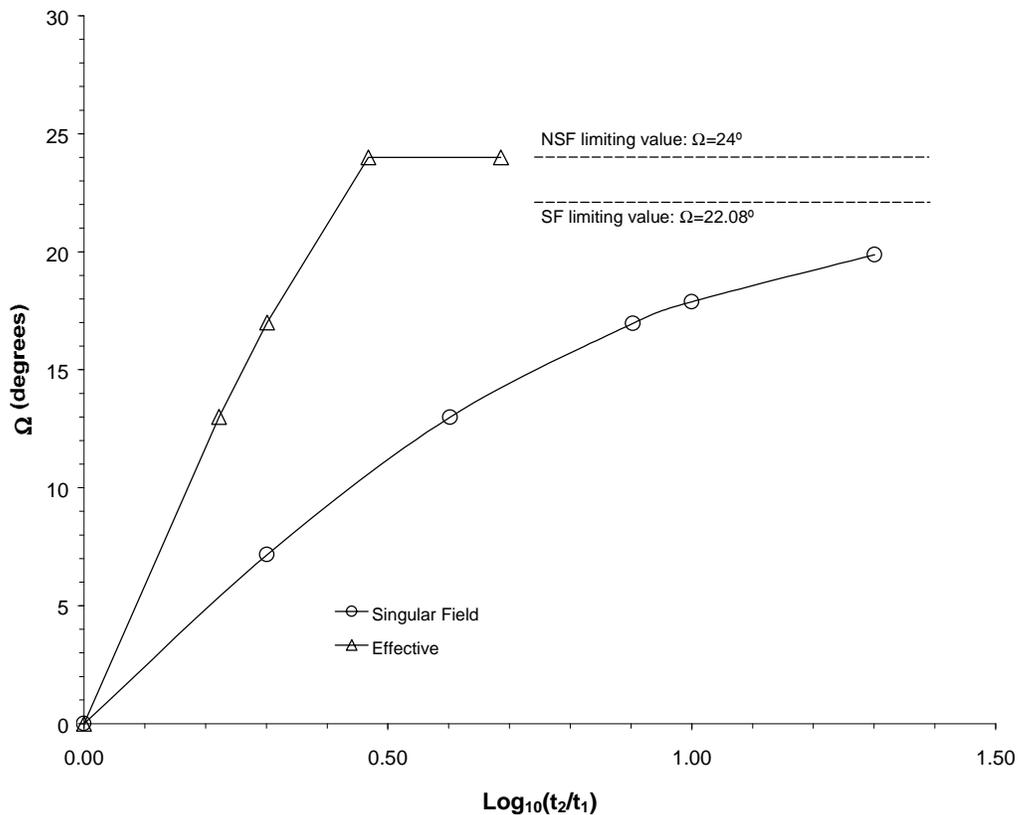

FIGURE 23. Ω VERSUS THICKNESS RATIO

36

6. GENERAL APPLICATION OF THE METHOD.

The work remaining to be done before this method can be used in general application is to assess whether the effective mode mix parameter obtained from the unidirectional samples can be used for all layups and interfaces, regardless of the test specimen stacking sequence. Preliminary test results [41] indicate that this method will be valid for 0/0, θ/θ, and θ/-θ interfaces, and based on this success, it is expected that it will be equally valid for all interfaces. However, as described in reference 1, there is some possibility that the definition of the effective mode mix parameter will need to be expanded to account for the [A-B-D] matrices of the various regions comprising the crack tip element, as well as for the orientations of the plies immediately adjacent to the delamination. Work in this area is currently being performed. Specifically, a second material is being tested, and for both materials, delamination growth under a variety of in-plane and bending loadings is being examined for a variety of interfaces and a variety of thickness ratios of the two cracked regions. Emphasis is on delamination between plies in the (0/±45/90) family, as these are the primary orientations used in practical applications. In addition to the above, a streamlined methodology is being evaluated that significantly reduces the amount of testing that is necessary to determine Ω-effective. Finally, the method will be applied to typical aircraft structural geometries, and failure predictions will be compared to the results of the corresponding structural test. All of these results will be presented in Part II, scheduled to be published in 2001.

7. CONCLUSIONS.

An engineering methodology has been presented for predicting delamination growth in laminated structures. There are two main components to this methodology. First, the toughness versus mode mix relation, and the definition of mode mix itself, is determined experimentally. The definition of mode mix is found from the results of a series of delamination toughness tests and is obtained within the construct of a crack tip element analysis. Second, the structure of interest is analyzed using the crack tip element analysis and the experimentally determined definition of mode mix and then delamination growth assessments are performed. Note that this approach obviates the need for locally detailed two- and three-dimensional finite element analyses.

The need for the delamination growth prediction methodology described herein is clear. For certain laminated materials, it has been conclusively demonstrated that the classical, LEFM, singular field-based approach will *not* accurately predict delamination growth [3-6]. In fact, considering the size of the crack tip damage in laminated composites in comparison to the characteristic dimension that scales the near-tip field (generally ply thickness), it is likely that the classical approach will not work for the majority of materials that are currently being used or that will be used in the near future. For these materials, the approach described herein allows a natural definition of mode mix to be determined for each material system. In these cases, mode mix is implicitly defined in terms of plate theory based quantities (N_c, N_c^y, and M_c) that fully describe the loading at the crack tip, yet which are insensitive to the details of any near-tip damage. Alternatively, for those materials where a singular field-based mode mix decomposition is valid, the above approach will reduce to the classical solution. As such, the approach described herein is believed to hold great promise for a successful predictive methodology for delamination of current and future laminated composites.

8. REFERENCES.

1.   Davidson, B.D., Hu, H., and Schapery, R.A., "An Analytical Crack Tip Element for Layered Elastic Structures," *Journal of Applied Mechanics*, Vol. 62, 1995, pp. 294-305.

2.   O'Brien, T.K., "Towards a Damage Tolerance Philosophy for Composite Materials and Structures," *Composite Materials: Testing and Design (Ninth Volume),* ASTM STP 1059, S.P. Garbo, Ed., American Society for Testing and Materials, 1990, pp. 7-33.

3.   Kinloch, A.J., Wang, Y., Williams, J.G., and Yayla, P., "The Mixed-Mode Delamination of Fibre Composite Materials," *Composites Science and Technology,* Vol. 47, 1993, pp. 225-237.

4.   Hashemi, S., Kinloch, A.J., and Williams, J.G., "Mixed-Mode Fracture in Fiber-Polymer Composite Laminates," *Composite Materials: Fatigue and Fracture (Third Volume)*, ASTM STP 1110, T.K. O'Brien, Ed., American Society for Testing and Materials, 1991, pp. 143-168.

5.   Charalambides, M., Kinloch, A.J., Wang, Y., and Williams, J.G., "On the Analysis of Mixed-Mode Failure," *International Journal of Fracture*, Vol. 54, 1992, pp. 269-291.

6.   Davidson, B.D., Fariello, P.F., Hudson, R.C., and Sundararaman, V., "Accuracy Assessment of the Singular Field-Based Mode Mix Decomposition Procedure for the Prediction of Delamination," *Thirteenth ASTM Symposium on Composite Materials: Testing and Design*, ASTM STP 1242, S.J. Hooper, Ed., American Society for Testing and Materials, 1997, pp. 109-128.

7.   Schapery, R.A. and Davidson, B.D., "Prediction of Energy Release Rate for Mixed-Mode Delamination Using Classical Plate Theory," *Applied Mechanics Reviews*, Vol. 43, No. 5, 1990, pp. S281-S287.

8.   Hu, H., "Analytical Determination of Energy Release Rate and Mode Mix for Interfacial Cracks," Ph.D. dissertation, Department of Mechanical, Aerospace and Manufacturing Engineering, Syracuse University, December 1995.

9.   Dundurs, J., "Mathematical Theory of Dislocations," American Society of Mechanical Engineering, 1969.

10.   Suo, Z., "Singularities, Interfaces and Cracks in Dissimilar Anisotropic Media," *Proceedings of the Royal Society of London*, A427, 1990, pp. 331-358.

11.   Whitney, J.M., "Structural Analysis of Laminated Anisotropic Plates," Technomic, 1987.

12.   Rice, J.R., "Elastic Fracture Mechanics Concepts for Interfacial Cracks," *Journal of Applied Mechanics*, Vol. 55, 1988, pp. 98-103.

13. Davidson, B.D., "Prediction of Delamination Growth in Laminated Structures," *Failure Mechanics in Advanced Polymeric Composites*, AMD-Vol. 196, G.A. Kardomateas and Y.D.S. Rajapakse, eds., American Society of Mechanical Engineers, 1994, pp. 43-65.

14. Davidson, B.D., "Prediction of Energy Release Rate for Edge Delamination Using a Crack Tip Element Approach," *Fifth Symposium on Composite Materials: Fatigue and Fracture*, ASTM STP 1230, R.H. Martin, ed., American Society for Testing and Materials, 1995, pp. 155-175.

15. Davidson, B.D. and Krafchak, T.M., "Analysis of Instability-Related Delamination Growth Using a Crack Tip Element," *AIAA Journal*, Vol. 31, No. 11, 1993, pp. 2130-2136.

16. Chai, H., Babcock, C.D., and Knauss, W.G., "One Dimensional Modeling of Failure in Laminated Plates by Delamination Buckling," *International Journal of Solids and Structures*, Vol. 17, 1981, pp. 1069-1083.

17. Yin, W.L., "The Effects of Laminated Structure on Delamination Buckling and Growth," *Journal of Composite Materials*, Vol. 22, 1988, pp. 502-517.

18. Davidson, B.D. and Ferrie, C.H., "Effect of Stretching-Shearing Coupling on Instability-Related Delamination Growth," *Composite Structures*, Vol. 29, No. 4, 1994, pp. 383-392.

19. Davidson, B.D., "Energy Release Rate Determination for Edge Delamination in Laminates Subjected to Combined In-Plane, Bending and Hygrothermal Loading - Part I: Delamination at a Single Interface," *Journal of Composite Materials*, Volume 28, No. 11, 1994, pp. 1009-1031.

20. Davidson, B.D., "Energy Release Rate Determination for Edge Delamination in Laminates Subjected to Combined In-Plane, Bending and Hygrothermal Loading - Part II: Two Symmetrically Located Delaminations," *Journal of Composite Materials*, Volume 28, No. 14, 1994, pp. 1371-1392.

21. O'Brien, T. K., Raju, I. S., and Garber, D. P., "Residual Thermal and Moisture Influences on the Strain Energy Release Rate Analysis of Edge Delamination," *Journal of Composite Technology and Research*, Summer 1986, pp. 37-47.

22. Raju, I.S., Crews, J.H. Jr., and Aminpour, M.A., "Convergence of Strain Energy Release Rate Components for Edge-Delaminated Composite Laminates," *Engineering Fracture Mechanics*, Vol. 30, No. 3, 1988, pp. 383-396.

23. Martin, R.H., "Delamination Onset in Polymeric Composite Laminates under Thermal and Mechanical Loads," *High Temperature and Environmental Effects on Polymeric Composites*, ASTM STP 1174, C.E. Harris and T.S. Gates, eds., American Society for Testing and Materials, 1993, pp. 39-65.

24. Davidson, B.D. and Hu, H., "Effect of Interlayer Modulus on Fracture Mode Ratio for Interleaved Composite Laminates," *Engineering Fracture Mechanics*, Vol. 52, No. 2, 1995, pp, 243-253.

25. Davidson, B.D., "An Analytical Investigation of Delamination Front Curvature in Double Cantilever Beam Specimens," *Journal of Composite Materials*, Vol. 24, No. 11, 1990, pp. 1124-1137.

26. Davidson, B.D., Krüger, R., and König, M., "Three Dimensional Analysis and Resulting Design Recommendations for Unidirectional and Multidirectional End-Notched Flexure Tests," *Journal of Composite Materials*, Vol. 29, No. 16, 1995, pp. 2108-2133.

27. Rybicki, E.F. and Kanninen, M.F., "A Finite Element Calculation of Stress Intensity Factors by a Modified Crack Closure Integral," *Engineering Fracture Mechanics*, Vol. 9, 1977, pp. 931-938.

28. Wang, J.T., Raju, I.S., Davila, C.G., and Sleight, D.W., "Computation of Strain Energy Release Rates for Skin-Stiffener Debonds Modeled with Plate Elements," AIAA paper 93-1501, Presented at the *34th AIAA/ASME/ASCE/AHS/ASC Structures, Structural Dynamics and Materials Conference*, 1993.

29. Williams, J.G., "On the Calculation of Energy Release Rates for Cracked Laminates," *International Journal of Fracture*, Vol. 36, 1988, pp. 101-119.

30. ASTM Standard D5228-94, "Standard Test Method for Mode I Interlaminar Fracture Toughness of Unidirectional Reinforced Polymer Matrix Composites," DCB Standard, American Society for Testing and Materials, 1994.

31. Broek, D., "Elementary Engineering Fracture Mechanics," Martinus Nijhoff Publishers, 1982.

32. Russell, A.J. and Street, K.N., "Factors Affecting the Interlaminar Fracture Energy of Graphite/Epoxy Laminates," *Progress in Science and Engineering of Composites*, ICCM-IV, T. Hayashi, K. Kawata, and S. Umekawa, eds., Tokyo, 1982, pp. 279-286.

33. Davidson, B.D., Krüger, R., and König, M., "Three Dimensional Analysis and Resulting Design Recommendations for Unidirectional and Multidirectional End-Notched Flexure Tests," *Journal of Composite Materials*, Vol. 29, No. 16, 1995, pp. 2108-2133.

34. Davidson, B.D., Altonen, C.S., and Polaha, J.J., "Effect of Stacking Sequence on Delamination Toughness and Delamination Growth Behavior in Composite End-Notched Flexure Specimens," *Composite Materials: Testing and Design (Twelfth Volume)*, ASTM STP 1274, C.R. Saff and R.B. Deo, eds., American Society for Testing and Materials, 1996, pp. 393-413.

35. O'Brien, T.K., Murri, G.B., and Salpekar, S.A., "Interlaminar Shear Fracture Toughness and Fatigue Thresholds for Composite Materials," *Composite Materials: Fatigue and*

36.   *Fracture, Second Volume*, ASTM STP 1012, P.A. Lagace, ed., American Society for Testing and Materials, 1989, pp. 222-250.

37.   Davidson, B.D., Krüger, R., and König, M., "Three Dimensional Analysis of Center Delaminated Unidirectional and Multidirectional Single Leg Bending Specimens," *Composites Science and Technology*, Vol. 54, No. 4, 1995, pp. 385-394.

38.   Sundararaman, V. and Davidson, B.D., "New Test Methods for Determining Fracture Toughness as a Function of Mode Mix for Bimaterial Interfaces," *Application of Fracture Mechanics in Electronic Packaging and Materials, EEP-Vol. 11/MD-Vol. 64*, T.Y. Wu, W.T. Chen, R.A. Pearson, and D.T. Read, eds., American Society of Mechanical Engineers, 1995, pp. 141-154.

39.   Reeder, J. and Crews, J., "The Mixed-Mode Bending Method for Delamination Testing," *AIAA Journal*, Vol. 28, No. 7, 1990, pp. 1270-1276.

40.   Reeder, J.R. and Crews, J.H. Jr., "Redesign of the Mixed-Mode Bending Delamination Test to Reduce Non-Linear Effects," *Journal of Composites Technology and Research*, Vol. 14, No. 1, 1992, pp. 12-19.

41.   Bhashyam, S. and Davidson, B.D., "Evaluation of Data Reduction Procedures for the Mixed Mode Bending Test," *AIAA Journal*, Vol. 35, No. 3, 1997, pp. 546-552.

42.   Polaha, J.J., Davidson, B.D., Hudson, R.C., and Pieracci, A., "Effects of Mode Ratio, Ply Orientation and Precracking on the Delamination Toughness of a Laminated Composite," *Journal of Reinforced Plastics and Composites*, Vol. 15, No. 2, 1996, pp. 141-173.